Global evaluation of ELMv1-CNP and the role of the phosphorus cycle in the historical terrestrial carbon balance

Xiaojuan Yang[1*], Peter Thornton[1], Daniel Ricciuto[1], Yilong Wang[2,3], Forrest Hoffman[4]

[1]Environmental Sciences Division, Oak Ridge National Lab, Oak Ridge, TN 37831, USA

[2]Key Laboratory of Land Surface Pattern and Simulation, Institute of Geographic Sciences and Natural Resources Research, Chinese Academy of Sciences, Beijing, China

[3]Laboratoire des Sciences du Climat et de l'Environnement, CEA-CNRS-UVSQ- Université Paris Saclay, 91191, Gif-sur-Yvette CEDEX, France

[4]Computational Sciences & Engineering Division, Oak Ridge National Lab, Oak Ridge, TN 37831, USA

Corresponding Author:

Phone: 865-5747615
E-mail: yangx2@ornl.gov

Abstract

The importance of carbon (C)-nutrient interactions to the prediction of future C uptake has long been recognized. The Energy Exascale Earth System Model (E3SM) land model (ELM) version 1 is one of the few land surface models that include both N and P cycling and limitation (ELMv1-CNP). Here we provide a global scale evaluation of ELMv1-CNP using International Land Model Benchmarking (ILAMB) system. We show that ELMv1-CNP produces realistic estimates of present-day carbon pools and fluxes. Compared to simulations with optimal P availability, simulations with ELMv1-CNP produces better performance, particularly for simulated biomass, leaf area index (LAI), and global net C balance. We also show ELMv1-CNP simulated N and P cycling are in good agreement with data-driven estimates. We compared ELMv1-CNP simulated response to CO_2 enrichment with meta-analysis of observations from similar manipulation experiments. We show that ELMv1-CNP is able to capture the field observed responses for photosynthesis, growth, and LAI. We investigated the role of P limitation in the historical balance and show that global C sources and sinks are significantly affected by P limitation, as the historical CO_2 fertilization effect was reduced by 20% and C emission due to land use and land cover change was 11% lower when P limitation was considered. Our simulations suggest that introduction of P cycle dynamics and C-N-P coupling will likely have substantial consequences for projections of future C uptake.

1. Introduction

The recent global carbon (C) budget showed that over the last half century global fossil CO_2 emissions have increased from about 3 Pg C/yr in 1960s to about 9.5 PgC/yr in the last decade (Friedlingstein et al., 2019). It has also been shown that land ecosystems play important roles in controlling the fractions of CO_2 emissions that remain in the atmosphere by taking up about 29% of total emissions (Le Quéré et al., 2018). Large uncertainties remain on the net land-atmosphere C exchange, mainly due to difficulties in quantifying the complex C cycle processes such as CO_2 fertilization effects, responses of carbon fluxes to temperature and precipitation variation, and C emissions associated with land use and land cover change (LULCC). These uncertainties will very likely hamper our ability to predict the future trajectories of atmospheric CO_2.

One of the important uncertainties relates to our understanding of C-nutrient interactions and nutrient limitation and how they are represented in models. The importance of nitrogen (N) availability to predicted land C storage has been long recognized (Hungate et al., 2003). Although there were only two models in CMIP5 (the fifth phase of the Coupled Model Intercomparison Project) that accounted for N dynamics and N limitation (Thornton et al., 2007; Thornton et al., 2009; Arora et al., 2013), many ESMs participating in CMIP6 (the Coupled Model Intercomparison Project phase 6) are now including N cycle and C-N interactions (Davies-Barnard et al., 2020; Lawrence et al., 2019; Goll et al., 2017a; Smith et al., 2014; Sellar et al., 2019). The comparisons between these models have been summarized in Arora et al. (2020) and Davies-Barnard et al. (2020). In recent years, significant efforts have also gone into understanding phosphorus (P) cycle dynamics and the role of P limitation in land C storage (Jiang et al., 2019; Hou et al., 2020; Reed et al., 2015; Wieder et al., 2015b; Sun et al., 2017). Increasing numbers of models have developed the capability to include P cycle processes and C-N-P interactions (Wang et al., 2010; Goll et al., 2012; Thum et al., 2019; Goll et al., 2017b; Yang et al., 2014; Yang et al., 2019; Sun et al., 2021). It has been shown that considering P cycle dynamics and C-N-P interactions improves process representation and model fidelity compared with observational and experimental data in most models (Goll et al., 2017b; Yang et al., 2014).

Model simulations have also demonstrated the importance of P limitation to land C uptake (Zhang et al., 2014; Goll et al., 2012; Yang et al., 2016; Yang et al., 2019; Sun et al., 2021). Using an ensemble of 14 terrestrial ecosystem models to simulate the planned free-air CO_2 enrichment experiment AmazonFACE, Fleischer et al. (2019) showed that P availability reduced the projected CO_2-induced C sink by about 50% compared to estimates from models assuming no phosphorus limitation. Taken together, understanding and representation of the role of P cycle dynamics in affecting terrestrial C balance is essential for the prediction of future terrestrial carbon uptake and atmospheric CO_2 concentration.

Field and modeling studies have shown that forest productivity tends to increase with increasing soil phosphorus availability (Vicca et al., 2012; Aragão et al., 2009; Wang et al., 2010). Despite these recent efforts, P cycle dynamics and C-N-P interactions are not yet included in most CMIP6 models. The Energy Exascale Earth System Model(E3SM) is one of the few models that have been developed a coupled C-N-P capability in the land component in CMIP6 (Burrows et al., 2020). The land model in E3SM, herein referred to as ELMv1-CNP, has been first applied in the Amazon region to test its capability and to evaluate the importance of P limitation in this region (Yang et al., 2019). Yang et al. (2019) provides an in-depth evaluation of ELMv1-CNP for the Amazon rainforest using field observational data, with a focus on how the introduction of P cycle dynamics and P limitation improved model simulated spatial variation of productivity. They show that effects of P limitation on C sources and sinks in the Amazon region are significant, reducing simulated CO_2 fertilization of new carbon uptake by as much as 31%.

This study expands the analysis in the Amazon region to the global scale and has two main aims: (1) to provide an evaluation of ELMv1-CNP performance on the global scale using both observational and experimental data, and (2) to quantify the role of P cycle dynamics and P limitation in affecting simulated C sources and sinks globally. We first evaluate the performance of ELMv1-CNP using the ILAMB benchmarking system (Collier et al., 2018), which has been widely used in the evaluation of land surface models and ESMs (Lawrence et al., 2019; Bonan et al., 2019; Zhu et al., 2019; Friedlingstein et al., 2019). We then evaluate ELMv1-CNP simulated N and P pools and fluxes with an observation-based

dataset. Realizing that the static benchmarking may not help constrain future model projections, we further evaluate ELMv1-CNP using experimental manipulations of atmospheric CO_2. Finally, we take advantage of the P-enabled capability in ELMv1-CNP to quantify the effect of P dynamics on the simulated ecosystem responses to increasing atmospheric CO_2, increasing N deposition, LULCC, and climate change on the global scale.

2. Method

2.1 Model Overview

ELMv1-CNP is based on the Community Land Model version 4.5 (CLM4.5), which includes coupled C-N biogeochemistry from CLM4 (Thornton et al., 2007) and improvements to canopy photosynthesis, soil biogeochemistry and representation of nitrogen cycle dynamics (Koven et al., 2013; Bonan et al., 2011; Oleson et al., 2013). Recognizing the critical role of the tropical forests in the global carbon cycle and C-climate interactions and the important role of P cycle dynamics and P limitation in tropical forests, we implemented a fully prognostic P cycle and C-N-P interactions into ELMv1-CNP, enabling ELMv1-CNP to be one of the few land surface models that include both N and P cycle dynamics and limitation. The main model features include (1) a fully prognostic P cycle tracking various soil inorganic P pools, vegetation P pools, litter and soil organic P pools (2) the representation of P limitation on plant productivity and litter and soil organic matter decomposition based on a supply-demand approach (3) resolving N vs P limitation using the Liebig law (4) the vertically-resolved soil inorganic and organic P dynamics (5) the decoupling of P cycle from C and N cycle during decomposition due to phosphatase activity (6) the representation of adsorption-desorption dynamics based on soil order.

Besides the P cycling processes, the other important difference of ELMv1-CNP from CLM4.5 is the removal of instantaneous downregulation of photosynthesis from nutrient limitation. Instead, longer-term downregulation of productivity is enabled through the implementation of C, N, and P nonstructural vegetation storage pools. In CLM4.5, nutrient limitation is calculated at each time step as a function of potential GPP, stoichiometry of plant tissues, and nitrogen uptake. Any “excess” carbon due to nitrogen limitation is

187 immediately released to the atmosphere through instantaneous downregulation. This
188 nutrient limitation can be highly variable over time and affects diurnal and seasonal cycles
189 of gross primary productivity, which is not consistent with flux tower observations (Ghimire
190 et al., 2016) or with short-term elevated CO_2 experiments that were done with and without
191 nutrient fertilization (Metcalfe et al., 2017). In the current model, competition for available
192 nutrients and plant uptake still occur every timestep given instantaneous demand that is a
193 function of plant GPP and microbial nutrient immobilization (Oleson et al.,
194 2013). However, nutrients taken up by plants are now first allocated to non-structural N
195 and P storage pools instead of directly to structural pools. Nutrient limitation to allocation
196 is determined by comparing plant nutrient demand (given GPP and stoichiometry) and the
197 nutrient availability from the non-structural nutrient pools, which is a function of the pool
198 size in relation to long-term demand. The "excess" carbon flux, which cannot be allocated
199 due to nutrient limitation, is directed to the non-structural plant carbon (NSC) pool instead
200 of downregulating GPP. This pool respires to the atmosphere with a given turnover time.
201 Details about the representation of NSC can be found in the supporting information (Text
202 S1)

203 The model version used in this study is the publicly released ELM v1 and can be
204 downloaded along with all the parameter files at https://github.com/E3SM-Project/E3SM.
205 In this version of the model, the fire module is activated by default. The soil erosion module
206 is not activated. We assume soil C, N, and P cycling can take place to the 3.8m depth as the
207 assumption in CLM4.5 (Koven et al., 2013). We also provide the key model parameters in
208 Table S1 (PFT specific) and Table S2 (soil order specific). We note that only leaf parameters
209 vary with PFT, but we include all other tissues in Table S1 to provide all parameters in the
210 consistent format.
211

212 **2.2 Simulations**

213 The simulations presented here were first spun up to bring C, N, and P pools to
214 equilibrium by recycling the GSWP3 (Global Soil Wetness Project Phase 3) climate forcing
215 data (http://hydro.iis.u-tokyo.ac.jp/GSWP3/) between 1901-1920, along with constant

atmospheric CO_2, N deposition and land cover type at year 1850. Spinup was accomplished through two steps: accelerated decomposition (AD) spinup and regular spinup. We ran the model for 250 years in the AD spinup mode. The purpose of the AD spinup is to accelerate the decomposition process and speed up the spinup process of the carbon and nutrient cycles. The AD spinup procedure was modified from that originally described by Thornton and Rosenbloom (2005), which used spatially invariant acceleration factors to accelerate decomposition in soil organic matter (SOM) pools. Here we updated the AD spinup by including the impacts of temperature and soil moisture on the acceleration factor. This resulted in higher acceleration factors in cool and/or dry climates, which are typically slower to achieve steady state. In addition, vegetation dead stem and coarse root mortality were accelerated by a factor of 10 to achieve steady state biomass more quickly. The factor of 10 was chosen to have a good balance between faster acceleration and the disequilibrium between accelerated and non-accelerated steady states that requires a longer regular spinup following Koven et al. (2013). In the AD spinup, supplemental soil mineral P was applied for the entire simulation such that there was no P limitation on C and N dynamics. During the transition between AD spinup and regular spinup, we initialized the soil inorganic pools using global P maps developed by (Yang et al., 2013). For the grid cells that don't have values in Yang et al. (2013), we applied the nearest neighbor method to estimate the values. Since the P cycle involves both biological and geochemical processes that occur on geological time scales, the initialization of P pools provides some reasonable estimates of soil P pools without running the model for millions of simulated years. More details regarding the rationale of using the developed P maps for initialization can be found in Yang et al. (2013). We then ran normal spinup for 600 years with active C, N, and P coupled biogeochemistry until C, N, and P pools reached equilibrium. The criteria for equilibrium are for global total NEE less than 0.1 PgC/yr averaged over 100 years, the threshold recommended for the C4MIP (Jones et al., 2016). We also ran a control simulation between 1850-2010 as a continuation of the normal spinup. We added the time series of labile P, secondary mineral P and occluded P for the control simulation (Fig. S1). There are very little changes in the inorganic P pools during the 161 years control simulation

suggesting that these pools can be considered in equilibrium for the time scale of our interest.

After the model was spun up, we ran the global historical transient simulations (1850–2010) at 0.5 degree spatial resolution using GSWP3 v2 climate forcing data, along with historical transient atmospheric CO_2 concentration, N deposition, land use and land cover change that are part of the CMIP6 protocols (https://luh.umd.edu/data.shtml). Input data and references are summarized in Table S3. We also ran a suite of single-factor simulations to examine the individual effects of changing environmental factors (atmospheric CO_2, land use and land cover change, climate, and nitrogen deposition, Table 1). In addition to the ELM v1 simulations with a fully active P cycle, we also performed historical transient and single-factor simulations with P limitation switched off (supplementing P availability to fully meet demand at each grid cell and for each timestep so there is no P limitation on productivity and decomposition). We denoted the default ELM v1 simulations that have an active P cycle as the CNP configuration (ELMv1-CNP) and simulations assuming no P limitation as the CN configuration (ELMv1-CN).

We also performed one additional simulation where we initiated a global step increase of atmospheric CO_2 concentration, by +200ppm, starting from 2001 and continuing through 2010. These simulations are designed to mimic the Free Air CO_2 Enrichment (FACE) experiments (Ainsworth and Long, 2005). To quantify model sensitivities to elevated CO_2, we calculated the effect size (treatment divided by control) over the10 years of simulation (2001-2010). We then evaluated model sensitivities to elevated CO_2 against meta-analysis from FACE experiments (Ainsworth and Long 2005).

All of the simulations are summarized in Table 1.

2.3. ILAMB

We used the International Land Model Benchmarking system (Collier et al., 2018; Luo et al., 2012; Hoffman et al., 2017) to assess the model performance. JLAMB was designed to use a wide array of observational data to constrain model results, including various land carbon pools and fluxes, inferred CO_2 concentration variability, and functional relationships.

Deleted: saturation (e. g. no P limitation on plant productivity or decomposition)

Formatted: Subscript

Deleted: The ILAMB package is a powerful tool for systematic evaluation of land model performance through comparison with observational data for biogeochemistry, hydrology, radiation and energy, and climate forcing.

Deleted: It

Deleted:

Formatted: Subscript

For each variable, ILAMB scores model performance for period mean, bias, root-mean-square error (RMSE), spatial distribution, interannual coefficient of variation, seasonal cycle, and long-term trend. These scores are aggregated into an overall score representing multiple aspects of model performance for each variable. These aggregated absolute scores are then used to calculate the relative score, which indicates the relative performance of each model with respect to other models used in the same analysis. The observational datasets used for the evaluation of carbon cycle in ILAMB are listed in Table S4.

In order to understand how the implementation of P cycling dynamics affects model performance, we evaluated the performance of both ELMv1-CNP and ELMv1-CN. In order to provide a context in terms of model performance in ILAMB, we provide the ILAMB evaluation of several other land models included in the Land Surface, Snow and Soil moisture Model Intercomparison Project (LS3MIP) as part of CMIP6 (https://www.wcrp-climate.org/wgcm-cmip/wgcm-cmip6). LS3MIP includes a collection of model experiments including both offline land model experiments and coupled experiments (Van Den Hurk et al., 2016). We used the results from the offline land model experiments. Like our simulations, these experiments were performed at 0.5by0.5 spatial resolution and using the GSWP3 forcing data. Other model configurations in LS3MIP are identical to that used in CMIP6 historical simulations, which we used for the simulations in this study.

2.4. GOLUM-CNP

Since there is no nutrient cycle metrics in ILAMB, we also compared major N and P pools and fluxes along with nutrient use efficiencies from ELMv1-CNP with the data-driven estimates of N and P pools and fluxes from the Global Observation-based Land-ecosystems Utilization Model of Carbon, Nitrogen, and Phosphorus (GOLUM-CNP) (Wang et al., 2018). GOLUM-CNP combines data-driven estimates of N and P inputs and outputs and observed stoichiometric ratios with a steady-state diagnostic model, providing global steady-state N and P pools and fluxes for large biomes. Despite large uncertainties and the steady-state assumptions, GOLUM-CNP provides a global data-driven product that can be used to test

Deleted: ILAMB offers a variety of graphical diagnostics and tabular data to assist the user in understanding when, where, and to what degree model results deviate from observational data. …

nutrient cycles in land surface models. GOLUM-CNP has also been used in the evaluation of other land surface models (Sun et al., 2021).

3. Results

3.1 Evaluations of ELM v1 using ILAMB

ILAMB includes many metrics that cover water, energy, and carbon pools and fluxes on both regional and global scales. Fig. 1 shows ILAMB benchmarking scores for ELMv1-CNP and ELMv1-CN, along with several other land models in CMIP6, which are provided to contextualize ILAMB scores for ELMv1-CNP. The relative model performance scores are shown in Fig. 1, indicating which model version performs better with respect to others. The full results produced by the ILAMB package can be found at https://compy-dtn.pnl.gov/yang954/_build/.

Fig. 1 shows that the performance of ELMv1-CNP is comparable to other land models in CMIP6. ELMv1-CNP exhibits performance similar to CLM5 (CESM2) in terms of aggregated scores for carbon cycle metrics, while CLM5 shows better performance with respect to overall functional relationships, mainly due to a better score for functional relationship of burned area. The performance of each model varies for different variables. For example, ORCHIDEE land surface model in IPSL-CM6A-LR performs relatively well in inferred atmospheric carbon dioxide, leaf area index and GPP relationships.

Fig.1 also shows the comparison between ELM v1-CNP and ELM v1-CN, allowing us to quantify the impacts of including a prognostic P cycle and realistic P availability on model performance. For metrics in Fig. 1 that show the greatest differences between ELMv1-CNP and ELMv1-CN, the CNP version always has a higher score than CN. This is reflected in the relatively higher aggregated scores for carbon cycle variables and functional relationships in ELMv1 -CNP.

Fig. 2 shows the Global Net Ecosystem Carbon Balance metric in ILAMB for ELM v1-CNP and ELM v1-CN. The observational data sets for this metric are from the Global Carbon Project (Fig. 2a)(Le Quéré et al., 2016) and from the inversion-based estimate (Hoffman et

al., 2014), both providing global totals of land carbon accumulation but for different historical time period (1850-2010 for Hoffman et al., 2014 and 1959-2010 for Le Quere et l., 2016). The simulated global C balance by both ELMv1-CNP and ELMv1-CN are in the range of uncertainty of observational estimates, with ELMv1-CNP simulated historical global carbon accumulation being a better match with mean observational estimates, particularly after 1950. ELMv1-CN estimated a net accumulation of land carbon of 22 Pg C over the period 1850-2010, which is much higher than the mean observational estimate of - 8Pg C. ELMv1-CNP estimated land carbon accumulation of 7 Pg C.

Fig. 3 shows the spatial distribution of vegetation biomass for the benchmark data and model bias in ILAMB. Overall both ELMv1-CN and ELMv1-CNP tend to overestimate biomass, compared to this specific global product of biomass (GEOCARBON). The high bias in the tropical region is much reduced in ELMv1-CNP simulations (Fig. 3a, 3b and 3c). The better performance of ELMv1-CNP is also reflected in the spatial Taylor diagram for biomass (Fig. 3d).

Another important benchmark in ILAMB is the functional relationships between two variables, for example the relationship between GPP and precipitation and the relationship between annual mean LAI and precipitation. An accurate simulation of these relationships in addition to individual benchmarks is an indication that the models are representing the underlying processes correctly. ELMv1-CNP produces a better functional relationship compared to ELMv1-CN. For example, for the relationship between LAI and precipitation ELMv1-CN overestimated LAI, particularly in regions with high precipitation, while the ELMv1-CNP configuration shows an improved relationship (Fig. 4). The improvement of the functional relationship is mainly due to the improvement in high precipitation regions, e.g. lowland tropical forest regions. In these regions, inclusion of P dynamics and P limitation reduced simulated bias in GPP and LAI, therefore leading to better match with the observations.

3.2. Evaluation of N and P cycling in ELMv1-CNP

We evaluated simulated nutrient use efficiencies against that from GOLUM-CNP product on the biome level. Here we define nutrient use efficiency as the ratio between annual NPP and annual nutrient uptake (for both N and P), with NUE for nitrogen use efficiency and PUE for phosphorus use efficiency (Finzi et al., 2007). ELMv1-CNP simulated NUE is higher in temperate and boreal forests and lower in tropical grassland and tundra, which is consistent with GOLUM-CNP (Fig. 5a). Temperate grassland NUE and PUE in ELMv1-CNP are higher in distribution because of the higher variation in NPP allocation to non-structural carbon pools. ELMv1-CNP predicted higher NUE in tropical lowland forests than GOLUM-CNP. ELMv1-CNP simulated PUE is generally consistent with GOLUM -CNP (Fig. 5b). However, ELMv1-CNP simulated PUE in tropical forests is much lower than that from GOLUM-CNP.

We also evaluated ELMv1-CNP simulated N and P pools and major fluxes on the global scale for the period of 2001-2010 with the observationally derived products in GOLUM-CNP. Fig. S2 shows the comparison of N and P uptake from ELMv1-CNP and GOLUM-CNP at the biome level. ELMv1-CNP simulated plant N and P uptake is in agreement with GOLUM-CNP, with higher uptake fluxes in tropical forests and lower uptake in temperate and boreal forests. ELMv1-CNP simulated N uptake is lower in the tropical forests, compared to GOLUM-CNP (Fig. S2a). Conversely, simulated P uptake is higher than GOLUM-CNP estimates across the tropics (Fig. S2b).

3.2 Evaluations using CO_2 manipulation experiment

Relative to the control simulation, increasing atmospheric CO_2 concentration by 200ppm increased gross primary productivity by 23% (global mean) over the 10 years of simulation (2001-2010). Nearly all PFTs showed more than a 10% increase in productivity, with more significant increases occurring in tropical regions and middle latitudes (Fig. 6a). The modeled response ratio of NPP is also showing widespread increases, and on the global scale our results showed a 25.8% increase in NPP in response to CO_2 enrichment (Fig. 6b). The simulated increases in GPP and NPP also showed, to a large extent, translated into increases in vegetation carbon (Fig 6c), with a global average response ratio of 18%. The

Deleted: However,

Deleted: also

Formatted: Subscript

modeled response ratio of LAI is much smaller, a 5% increase globally (Fig 6d). The globally aggregated simulated effect size of CO_2 enrichment from ELMv1-CNP on GPP, NPP, LAI and NSC compare well to the observations from the meta-analysis (Fig. 7), particularly for GPP and LAI. ELMv1-CNP overestimated the responses of NPP. Both observations and simulations show large sensitivity of NSC to CO_2 enrichment, with larger variability in the model simulations.

Formatted: Subscript

3.3. Carbon, nitrogen and phosphorus pools and fluxes

3.3.1 Carbon budget

Major components of the global land C budget for present day (mean of 2001–2010) in ELMv1-CNP are shown in Fig 8a. These are from historical simulations with transient climate forcing, atmospheric CO_2 concentration, land use and land cover change, and N deposition. For the present day, model simulated total ecosystem C is 2588.73 Pg C, with about 22% stored in vegetation (575.45 Pg C), about 5% stored in litter and coarse wood debris (122.5 Pg C), and 73% stored in soil organic matter (1890.78 Pg C). Model simulated vegetation C is within the range of inventory-based estimates from IPCC AR5 (450–650 Pg C). Our simulated vegetation C is also comparable to or slightly higher than observational estimates from the literature: 455Pg C (GEOCARBON, (Avitabile et al., 2016; Santoro et al., 2015), 550±100 Pg C (Houghton, 2003), 560±94 Pg C (Defries et al., 1999), and 450 Pg C (Erb et al., 2018). Model simulated total soil C is within the range of estimates from IPCC AR5 (1500-2400 Pg C) and that from Jobbágy and Jackson (2000) (1750±250 PgC). Model simulated total soil C is lower than several other observational estimates from the literature: 2376-2456 (Batjes, 2014), 3000 Pg C (Köchy et al., 2015), which could be because ELMv1-CNP has yet to include an explicit representation of peatland carbon dynamics. As for the top 1m soil carbon, model simulated values of 1134.41 Pg C are within the range of estimates from the Harmonized World Soil Database (HWSD) (FAO/IIASA/ISRIC/ISSCAS/JRC, 2012) as reported by Todd-Brown et al. (2013) (890-1660 Pg C), but lower than the observational based estimate of 1462–1548 Pg C from Batjes (2014) and 1325 Pg C from Köchy et al. (2015). Model simulated litter C (22.9 Pg C) is lower than the observational based estimate: 68 Pg C

Formatted: Subscript

Deleted: .

(Matthews, 1997) and 43±3 Pg C (Pan et al., 2011). Model simulated coarse wood debris C stock (99.6 Pg C) is higher than the observational based estimate: 75 Pg C (Matthews, 1997) and 73±6 Pg C (Pan et al., 2011).

Deleted: 4

Deleted: 3

Model simulated present day GPP(134.15 Pg C/yr) is slightly higher than observational based estimate: 123±8 Pg C/yr (Beer et al., 2010), 119±6 Pg C/yr (Jung et al., 2011) and 123 PgC/yr (IPCC AR5), and lower than 150-175 Pg C/yr from Welp et al. (2011) that is derived based on oxygen isotopes of atmospheric CO_2. A recent study based on satellite data suggested a global GPP of 140 Pg C/yr for year 2007 (Joiner et al., 2018). The comparisons between simulated carbon pools and fluxes and available observations are also included in Table 2.

3.3.2. Nitrogen budget

The ELMv1-CNP estimated N budget for the present day (2001–2010) is summarized in Fig 8b. Compared to the C cycle, there are fewer observational estimates for N pools and fluxes. Most of the literature values are from other model simulations. Although not appropriate for direct model evaluation, these modeling estimates from the literature provide a broad context for us to evaluate our simulated pools and fluxes.

Model simulated vegetation N is 4.36 Pg N, which is comparable to the estimates from some other modeling studies: 3.8 Pg N (Zaehle et al., 2010), 5.3 Pg N (Xu and Prentice, 2008) and lower than the estimates of 16 Pg N(Lin et al., 2000) and 18 Pg N (Yang et al., 2009). Model simulated total soil organic matter N is 188.79 Pg N, which is reasonable considering the observational based estimate for 1m of 95 Pg N (Post et al., 1985) and 133–140 Pg N (Batjes, 2014). ELMv1-CNP estimated biological nitrogen fixation (BNF) of 89 TgN/yr is within the range of estimates from literature. Vitousek et al. (2013) estimated that global BNF ranges between 40–100 TgN/yr using a mass-balance approach. A meta-analysis by Davies-Barnard and Friedlingstein (2020) suggested that global inputs of BNF in natural ecosystems range between 52 and 130 TgN/yr, with a median global value of 88 TgN/yr. For the purpose of comparison, BNF estimates from CLM5 is 96.4 TgN/yr, slightly higher than

our estimate. The comparisons between simulated N pools and fluxes and available observations are also included in Table 2.

3.3.3 Phosphorus budget

The ELMv1-CNP estimated P budget for the present day (2001–2010) is summarized in Fig 8c. Very few observational data are available for P on the global scale. The only observation-based global product is the global P maps developed by (Yang et al., 2013). Model simulated vegetation P is 0.36 Pg P, which is comparable to the estimates from other modeling studies ranging from 0.23 to 3 Pg P (Goll et al., 2012; Wang et al., 2010; Jahnke, 1992). Model simulated soil organic P is 3.75 Pg P, which is slightly lower than previous studies 5.74 Pg P (Goll et al., 2012), 5-10 Pg P (Smil, 2000), and 8.6 Pg (Yang et al., 2013). Model simulated soil mineral P for the top 40cm and 60cm is 63.24 Pg P and 81.32 Pg P respectively, which are generally comparable to the estimate of 45 Pg P for top 50cm soil from Yang et al. (2013). The comparisons between simulated P pools and fluxes and available observations are also included in Table 2.

3.4. The effects of P limitation on historical carbon cycle

ELMv1-CNP calculates the extent of both N and P limitation for plant growth on the global scale (Figs. 9a and 9b). Generally speaking, P is a more limiting nutrient in tropical evergreen forests and savannas in South America and Africa, while N is more limiting in temperate regions (Fig. 9a). The ratio between the P limitation factor and N limitation factor illustrates the degree of N-P colimitation (Fig. 9b). N and P are co-limiting productivity in tundra, boreal forests, and deserts.

Fig. 10 shows the simulated spatial patterns of productivity and carbon storage and how they are affected by P dynamics and limitation. P dynamics strongly control land carbon uptake and storage, particularly in tropical regions. Globally NPP is highest in tropical evergreen forests and lower in middle to high latitude regions. Plant growth in tropical regions, however, is generally limited by P availability, particularly in the central

Deleted: In many parts of the world, both

Deleted:

Deleted: .

Moved (insertion) [1]

Deleted: 1

and eastern Amazon basin and tropical Africa. The reduced productivity due to P limitation translates into reduced vegetation carbon storage and soil carbon storage, with the exception of tropical savannas, where fire dynamics also play an important role in vegetation and soil carbon storage.

Fig. 11 shows the effects of P dynamics on historical global land carbon accumulation. The introduction of P dynamics leads to a 19.5% reduction in global C storage due to CO_2 fertilization between 1850 and 2010. The consideration of P dynamics also leads to a lower estimate of land use emissions on the global scale(143.89 PgC vs 161.21 PgC) as CNP simulations generally show lower initial vegetation biomass. Increasing N deposition generally leads to a small carbon accumulation between 1850 and 2010 in both CN and CNP simulations globally. With P limitation, however, the global carbon accumulation from N deposition is reduced by about a third. Climate, although responsible for the large seasonal and interannual variability of carbon fluxes, has only minor impacts on historical carbon accumulation on the global scale for both CN and CNP simulations. When changes of all environmental factors are considered, the impact of P dynamics on carbon accumulation is the balance between a smaller CO_2 fertilization effect and lower land use emissions, with the net effect being slightly lower historical carbon accumulation globally.

Deleted: 0

Moved up [1]: Fig. 11 shows the simulated spatial patterns of productivity and carbon storage and how they are affected by P dynamics and limitation. P dynamics strongly control land carbon uptake and storage, particularly in tropical regions. Globally NPP is highest in tropical evergreen forests and lower in middle to high latitude regions. Plant growth in tropical regions, however, is generally limited by P availability, particularly in the central and eastern Amazon basin and tropical Africa. The reduced productivity due to P limitation translates into reduced vegetation carbon storage and soil carbon storage, with the exception of tropical savannas, where fire dynamics also play an important role in vegetation and soil carbon storage. ¶

4. Discussions

4.1. ILAMB benchmarking

This study presents a global assessment of the ELMv1-CNP. Yang et al. (2019) evaluated the performance of ELMv1-CNP in the Amazon region using plot-level observations from the RAINFOR network and found that the model captures well the observed productivity and biomass gradient across the Amazon basin. Here we further evaluate the global model performance using the ILAMB benchmarking system – an open source land model evaluation system that is designed to assess model performance at site level, regional, and global scales in an integrated and comprehensive way.

We include several other land models in CMIP6 in our ILAMB analysis with the goal of providing a context for the performance of ELMv1-CNP. We found that ELMv1-CNP exhibits similar performance to other models. It is challenging to demonstrate a clear improvement or degradation for complex land surface models in ILAMB. For example, our analysis indicates that ELMv1-CNP performance is comparable to CLM5 in terms of the overall carbon cycle. Both ELMv1-CNP and CLM5 have a common ancestor CLM4.5, but they took very different approaches for further development. CLM5 had significant efforts undertaken in improving the representation of nitrogen cycle, while ELMv1-CNP was more focused on implementing a prognostic phosphorus cycle and C-N-P interactions. Model development activities in both models helped improved model performance through the lens of ILAMB but the sources of improvements are quite different. This highlights the need to include more process-level evaluations in ILAMB for the purpose of evaluating the impact of specific model improvements.

Although CLM5 and ELM-CNP perform similarly in terms of ILAMB scores, it is worth noting the unique role of P cycle dynamics in affecting C cycling and the importance of including P cycle limitation in earth system models for better prediction of carbon-climate feedbacks. The important role of soil P availability in affecting plant growth in tropical forests residing on highly weathered soils has long been recognized (Walker and Syers, 1976; Vitousek et al., 2010; Butler et al., 2018; Elser et al., 2007). Recent work has also explored how increasing demand for P may attenuate predicted increase in NPP conceptually by comparing potential demand with potential nutrient availably in the 21st Century (Wieder et al., 2015b; Sun et al., 2017). Increasing numbers of land models have incorporated P cycle dynamics and P limitations (Sun et al., 2021; Nakhavali et al., 2021). Although both N and P limitation acts through reducing NPP, it is critical to include P cycling explicitly in models since P cycle dynamics are very different from the N cycling dynamics. The primary input for P is through rock weathering, which make it a very much non-renewable nutrient for the terrestrial ecosystems, whereas N fixation, the primary input for N, is more biologically driven. P cycling involves the transformation of various forms of P through a series of biological, enzymatical and geochemical processes with the turnover

time ranging from seconds to millions of years. N cycle dynamics are relatively simpler, with two inorganic forms and mostly biological and enzymatical processes involved. In addition, the interactions between N and P cycling also points to the need to include P cycle explicitly in land models. Increasing numbers of studies have shown that biological N fixation could be constrained by soil P availability (Hungate et al., 2004; Reed et al., 2013; Barron et al., 2008; Edwards et al., 2006; Crews et al., 2000). On the other hand, studies have also shown that increases in N availability can promote phosphatase activity and enhance biochemical mineralization and therefore accelerate P cycling (Mcgill and Cole, 1981; Wang et al., 2007; Houlton et al., 2008; Olander and Vitousek, 2000; Treseder and Vitousek, 2001; Marklein and Houlton, 2012). We will continue refine and improve the representation of the C-N-P interactions in the future development of ELM.

Also, ILAMB, despite being a comprehensive benchmarking tool for land surface models, is limited in scope in terms of the benchmarking data included. For example, Quesada et al. (2012) found that the decreasing west-east gradient in productivity is mostly related to total soil P across the Amazon basin. Yang et al. (2019) show that consideration of soil P availability improved model simulated productivity, enabling the model to capture the productivity gradient from west to east across the Amazon basin. The problem is that this productivity gradient across the Amazon basin is not captured in ILAMB benchmark data so the "failure" of a CN model would not be captured by ILAMB.

We show that the model performance generally improved with realistic P availability through the implementation of a prognostic P cycle in ELM. Compared to ELMv1-CN, ELMv1-CNP simulated biomass has lower bias across the tropical regions as P limitation leads to lower productivity and hence lower biomass. ELMv1-CNP produces better ILAMB scores on the functional relationships between GPP, LAI and other forcing variables, mainly due to improved estimate of GPP and LAI in tropical regions. ELMv1-CNP also produces higher ILAMB scores for the integrated benchmarks such as global net ecosystem carbon balance and carbon dioxide concentration. We note that satisfactory performance for these two integrated metrics is most critical to a land model in ESMs as they are most relevant to the coupling between land ecosystems and radiatively-forced climate change.

ELMv1-CNP is not always better than ELMv1-CN from the benchmarks in the current ILAMB system. One of the benefits of a multi-metric analysis package like ILAMB is that we can compare performance at different levels of granularity, and it is rare that any one model has uniformly improved performance over any other single model on every fine-grained metric. By having multiple data sources for a given metric we can often see improvement against one data source and degradation compared to another for the same model output. For example, the ELMv1-CN model performs better than ELMv1-CNP for ecosystem respiration when comparing the Fluxnet metric, but ELMv1-CNP does better than ELMv1-CN for the GBAF metric on the same output variable. In the case of GPP and NEE, although ELMv1-CN is performing better or the same as ELMv1-CNP for both Fluxnet and GBAF metrics, the overall better scores of the ELMv1-CNP model for the relationship metrics connected to GPP give us more confidence that ELMv1-CNP is actually an improvement. Each metric has its own advantages and disadvantages, and there is still considerable subjectivity in how to interpret the multi-metric collection. For example, the site-level evaluations in iLAMB do not take into account site-specific disturbance histories, which can be an important driver of NEE variability over time at a given site.

Although the ILAMB benchmarking system is very useful for evaluating model performance from different aspects simultaneously, interpretation of ILAMB scores deserves extra caution with known observational bias considered. For example, ILAMB uses LAI estimated from remote sensing observations from the Moderate Resolution Imaging Spectroradiometer (MODIS) as benchmarking data, while studies have suggested that MODIS LAI may be biased low due to reflectance saturation in dense canopies in the tropical forests (Shabanov et al., 2005; Huete et al., 2002; Kobayashi and Dye, 2005). Another example is the observational data for biomass. There are significant differences between the “tropical” and “GlobalCarbon” datasets and the “GeoCarbon” dataset for tropical biomass, but they were given about the same default weight in the ILAMB scoring system. Mitchard et al. (2014) investigated the marked differences between different estimates of Amazon biomass and suggested the regional biases in some remote sensing

627 products might be due to the lack of consideration of ecological variation in tree wood
628 density and allometry. Further investigation of these datasets is needed to ensure the
629 quality of biomass benchmarking data.
630
631 The current version of ILAMB includes analysis of 28 variables using more than 60
632 datasets or data products. None of these variables, however, are directly related to nutrient
633 cycles. As more land surface models are implementing N and P dynamics, it is becoming
634 increasingly important to include metrics for nutrient stocks and fluxes. Davies-Barnard et
635 al. (2020) assessed five nitrogen-enabled land surface models in CMIP6 and called out the
636 need to have better constraints of nitrogen cycle processes. The need is equally urgent, if
637 not more, to synthesize more observations to better constrain the P cycle processes, as less
638 synthesized data are available for P. Encouragingly, recent studies have started to develop
639 observational datasets based estimate of N and P cycling on the global scale for model
640 evaluation, such as the GOLUM-CNP dataset we used in this study. We hope to highlight the
641 need and engage the broader community in developing additional nutrient datasets that
642 can be included in ILAMB.
643 Other metrics that would be useful are the responses from N and P addition
644 experiments. As Yang et al. (2014) showed, fertilization experiments at sites along the
645 Hawaii chronosequence provided a useful evaluation testbed to assess model simulated
646 responses to N and P fertilization effects. FACE experiments are useful for model evaluation
647 as shown here (section 4.2) and in other studies (Wieder et al., 2019; Davies-Barnard et al.,
648 2020). Warming studies that include an explicit focus on nutrient cycle responses will be
649 another good evaluation opportunity (Melillo et al., 2002). An existing challenge is to
650 provide a common protocol to use these types of experiments in the ILAMB benchmarking
651 system.
652
653 4.2 Evaluations using GOLUM-CNP
654
655 On the biome level ELMv1-CNP simulated nutrient use efficiencies are consistent with
656 the observation-based estimates from GOLUM-CNP. This indicates that the representation

of N and P cycling and C-N-P coupling is reasonable in ELMv1-CNP. In terms of nutrient uptake, both show the highest N and P uptake in tropical forests, due to the high N and P demand associated with high productivity. ELMv1-CNP predicted lower N uptake in the tropical forests, compared to GOLUM-CNP. Nutrient uptake in ELMv1-CNP is a function of nutrient availability and nutrient demand, with demand being determined by available carbon for allocation, allocation fractions to different plant tissues and plant tissue stoichiometry. The simulated NPP at the biome level matches well with NPP from GOLUM-CNP except for Tundra (Fig. S3). The different C:N and C:P stoichiometric ratios for vegetation tissues used in ELMv1-CNP and GOLUM-CNP could also contribute to the difference in . C:N ratios of leaf, wood, and fine root in GOLUM-CNP are all lower than ELMv1-CNP (21, 126, and 40 in GOLUM vs 30, 500, and 42 in ELMv1-CNP). This suggests for given amount of carbon allocation, N uptake would be lower in ELMv1-CNP. Soil P availability might be overestimated considering ELMv1-CNP estimated P leaching is much lower than the estimate of Wang et al. (2018), therefore leading to relatively higher P uptake in ELMv1-CNP. Differences in allocation factors could also be contributing to the differences in nutrient uptake between ELMv1-CNP and GOLUM-CNP. For example, the mean allocation fraction to fine root is higher in GOLUM-CNP compared to ELM-CNP, while allocation fraction to leaf is lower in GOLUM-CNP, particularly in forest ecosystems (Fig. S4 and S6). GOLUM-CNP also has higher NPP allocation fraction to woody biomass in boreal forests (Fig. S5)

Deleted: s

Deleted:

Deleted: The differences in nutrient uptake is therefore likely due to …t
t

Deleted: t

Deleted: different

Formatted: Font color: Text 1

Deleted: . C:P ratios of leaf, wood, and fine root in GOLUM-CNP also differ quite significantly from those in ELMv1-CNP (410, 5429, and 1250 in GOLUM vs 600, 3000, and 1000 in ELMv1-CNP). The relatively higher P uptake in ELMv1-CNP can be attributed in large part to the difference in dead wood C:P ratios.

4.3. Evaluations using CO_2 manipulation experiments

Our simulated large increase in GPP with CO_2 enrichment (23%) is in agreement with field observations that photosynthetic assimilation increased 28% under elevated CO_2 (Ainsworth and Long, 2005). Our simulated 26% increase in NPP is higher than the 17% increase in observed increase in dry matter production in the FACE experiments (Ainsworth and Long, 2005; Wieder et al., 2019). Our simulated 18% increase in biomass is higher than the estimates from Terrer et al. (2019), which provides a data-driven estimate of global CO_2 fertilization effect on biomass and show a relative increase in biomass of 12±3% for a 250

ppm CO_2 increase. A meta-analysis of woody plants responses to elevated CO_2 shows a mean effects of 22.3% on biomass (Baig et al., 2015). Among CLM4, CLM4.5 and CLM5, ELMv1-CNP is more comparable to CLM5 with a strong simulated response of GPP, NPP, and vegetation carbon in response to CO_2 enrichment, while CLM4 and CLM4.5 showed very weak CO_2 effects (Wieder et al., 2019).

The much stronger sensitivity of photosynthesis to elevated CO_2 in ELMv1-CNP is due to the removal of instantaneous downregulation of photosynthesis as a response to nutrient limitation. The instantaneous downregulation assumption in CLM4 and CLM4.5 has been shown to be inconsistent with experimental results (Metcalfe et al., 2017). Despite large uncertainty, it is encouraging that simulated NSC response to elevated CO_2 is largely consistent with the observational data (Fig. 7). The low sensitivity of LAI in ELMv1-CNP is also consistent with field observations. Our results suggest the assumption we made regarding the fate of photosynthate is reasonable. Yang et al. (2016) showed that enhanced phosphatase enzyme production response to increasing CO_2 could have important impacts on P availability and sustain forest productivity under elevated CO_2. In simulating the planned free-air CO_2 enrichment experiment AmazonFACE, ELMv1-CNP simulated phosphatase activity increased about 20% over 15 years (Fleischer et al., 2019). Here we show that introduction of NSC pools further improve the response of vegetation processes to changes in P availability and P limitation.

Our findings are consistent with field studies that show the strong increase of NSC under elevated CO_2 condition (eCO_2), particularly when nutrient availability is low (*Wong*, 1990; *Körner et al.* (2005). Several studies evaluating CLM4.5 using carbon isotope data also suggested that model performance would be better with the introduction of an NSC pool (Mao et al., 2016; Raczka et al., 2016; Duarte et al., 2017). However, large uncertainties remain regarding the turnover rate of the NSC pool. Further synthesis of field measurements on NSC in CO_2 enrichment experiments are needed to evaluate and constrain the representation of NSC in models.

Formatted: Subscript
Formatted: Subscript
Formatted: Subscript
Formatted: Subscript
Formatted: Subscript

Our simulated strong sensitivity of photosynthesis to CO_2 enrichment is consistent with recent studies that show large GPP growth during the twentieth century (Campbell et al., 2017; Haverd et al., 2020; Ehlers et al., 2015). Ellsworth et al (2017) also showed a large increase of photosynthesis in response to elevated CO_2 in a temperate forest FACE experiment.

The increased sensitivity of GPP and NPP to CO_2 enrichment in ELMv1-CNP, compared with the predecessors CLM 4 and CLM4.5, will very likely reduce the bias in the atmospheric fraction of human CO_2 emissions in previous coupled simulations as noted by Hoffman et al. (2014). In fact, CO_2 concentration metrics in ILAMB, which translate model simulated NEE into atmospheric CO_2 signal using an atmospheric transport model (Collier et al., 2018), is intended for the evaluation of this sensitivity. The inferred atmospheric CO_2 concentration from ELM v1 is very reasonable compared with observed NOAA flask data (Fig. S7 and S8).

4.4. Model estimated carbon, nitrogen, and phosphorus pools and fluxes

Global C, N, and P pools in our ELMv1-CNP simulation are in good agreement with recent independent global estimates, indicating that ELMv1-CNP is capable of simulating the contemporary C, N and P cycles. In Yang et al. (2019) it was shown that introduction of more realistic mortality processes improved the model representation of longitudinal spatial patterns of biomass across the Amazon basin. Here we show that an overall high bias in biomass production is corrected through limits of vegetation production in response to P availability, without compromising the improved spatial gradients obtained through the mortality mechanism. It is worth mentioning that our understanding of nutrient stocks and fluxes is much less advanced in comparison with the global C cycle. This has been increasingly acknowledged for the global N cycle as increasing numbers of land surface models have incorporated N cycle dynamics and C-N interactions (Zaehle et al., 2010; Wieder et al., 2019; Davies-Barnard et al., 2020; Smith et al., 2014; Sellar et al., 2019; Goll et al., 2017a; Gerber et al., 2010). Biological N fixation and N-use efficiency have been identified as the key processes that need to be better constrained for land surface models (Davies-Barnard et al., 2020).

Formatted: Subscript

Deleted: 8

Deleted: 9

Our understanding of P stocks and fluxes are even less advanced than that for the N cycle, as shown in this study and other modeling studies that include P as a limiting nutrient. This is mainly due to: (1) various forms of P with different level of availability for plants and microbes, (2) geochemical processes in conjunction with biological processes controlling P availability, and (3) technical challenges in measuring soil P. For example, Hedley fractionation data provide a comprehensive picture of different P forms in soils and has been used for model evaluation and/or initialization in all the land surface models that include a prognostic phosphorus cycle (Wang et al., 2010; Goll et al., 2012; Yang et al., 2014; Yang et al., 2019). However, this extraction method is time-consuming and challenging, and not many routine measurements have been made using this technique. As such, observational estimates of P pools and fluxes are extremely limited. Although recent global Hedley database development (Yang and Post, 2011; Hou et al., 2018) has been helpful in global model development and evaluation, more observational data on P stocks and fluxes are needed to better constrain P-enabled models.

4.5. Effects of accounting for the P cycle dynamics on simulated carbon balance

4.5.1. Spatial variation of nutrient limitation

Our simulated nutrient limitation pattern broadly agrees with the findings from Elser et al. (2007) which supports the generally accepted notion that tropical ecosystems residing on highly weathered soils are P limited (Walker and Syers, 1976; Lebauer and Treseder, 2008). A recent study that predicted spatial patterns of N and P limitation using the ratios of leaf N and P resorption efficiencies also found a shift from P limitation to N limitation with increasing latitude (Du et al., 2020). Lebauer and Treseder (2008) showed that N limitation is widespread, even in tropical regions. This is consistent with our model simulations which show that although P is more limiting in tropical forests, N is also a limiting nutrient. The geographic distribution of nutrient limitation is generally in agreement with that from Goll et al. (2012) and Wang et al. (2010). Goll et al. (2012) suggests that P limits C uptake mainly in low latitude regions and high latitudes, while N is

the limiting nutrient in temperate regions. It is worth mentioning that in Goll et al. (2012) N and P limitation generally have distinct geographic occurrence while this study suggests NP co-limitation occurs in many parts of the world. Wang et al. (2010) also showed that productivity in tropical forests and savanna is limiting by P, while most other biomes are limited by N. This is broadly consistent with our results but with a few key differences. Wang et al. (2010) suggests that P is the limiting nutrient for savannas, whereas our results show savannas are more limited by N. This may have to do with the lack of representation of fire disturbance in Wang et al. (2010). Savannas are subject to regular wildfires, which could have significant effects on nutrient cycle dynamics and nutrient limitation. For example, it has been suggested that while combustion causes significant gaseous losses of N from burned ecosystems, P is largely retained as ash (Herbert et al., 2003). Braakhekke et al (2017) also showed that there are strong losses of N due to fire. Furthermore, Wang et al. (2010) suggested that tropical forests are limited only by P, not by N, whereas our results indicate that N and P both limit tropical forest productivity, although P limitation is more dominant in most of the lowland tropical forests. This is consistent with a recent meta-analysis of nutrient fertilization experiments in tropical forests (Wright et al., 2018).

4.5.2. The implications for global carbon cycle and climate

Historical C accumulation is a result of many complex and sometimes counteracting processes controlling C fluxes and stocks (Lawrence et al., 2019), including accumulation of carbon on land due to CO_2 fertilization, accumulation due to nitrogen deposition, carbon fluxes due to climate variability and climate change, and losses and gains due to land cover conversion and regrowth following historical land cover changes (LULCC fluxes).Over the long term, two of the dominant processes controlling C accumulation in terrestrial ecosystems are C emissions due to LULCC and C uptake due to the CO_2 fertilization effect. P cycle dynamics have important impacts on both of these processes, but with opposite sign. Globally, considering P cycle dynamics leads to lower carbon emissions associated with deforestation by about 11% (161.21 Pg in CN vs 143.89 in CNP). Conversely, CO_2 fertilization at the global scale is reduced by 20% when P limitation is included during the

historical time period (134 Pg C vs 108 Pg C). In general, the ELMv1-CN simulation shows a CO_2 fertilization effect on biomass that is too strong, which leads to a stronger than observed carbon sink compared to observational constraints from both Hoffman et al. (2014) and Le Quere et al. (2016). ELMv1-CN simulation also produces stronger carbon emissions from LULCC due to having higher biomass compared to ELMv1-CNP. The CO_2 fertilization effect in the ELMv1-CN simulations is strong enough to overcome the LULCC losses with the net result being too large of a sink throughout the historical time period for the CN model. Both model configurations lose carbon too slowly due to LULCC in the period from 1850–1940, when compared to the Hoffman et al. (2014) global estimate. Both models also predict continued losses over the period 1940–1965, while the Hoffman et al. (2014) estimate switches from net carbon loss to net carbon accumulation around 1940. These are clearly shown in Fig. S9, which shows the time series of simulated change in land carbon storage in response to changes in CO_2, LULCC, N deposition, and climate during 1850-2010. The ELMv1-CN and ELMv1-CNP models are similar to many other CMIP6 models with respect to this bias in the timing of transition from net land carbon source to net land sink as shown in our ILAMB analysis of other land models in CMIP6.

Deleted: 7

We also note that, over the historical time period, P became more limiting as simulated historical C accumulations became increasingly divergent between CN and CNP simulations. This is mainly caused by stimulated plant productivity under higher atmospheric CO_2, which leads to higher plant demand for P that is not balanced by increased supply of newly mineralized P from the soil. This is consistent with other global modeling studies with explicit representation of P cycle dynamics (Goll et al., 2012; Zhang et al., 2014), as well as diagnostic studies that evaluated how CO_2 fertilization simulated by CMIP5 models could be constrained by soil P availability using a mass balance approach (Wieder et al., 2015b; Sun et al., 2017). Taken together, the limiting effect of P availability on C uptake will likely have substantial consequences for projections of future C uptake.

846 **4.6. Limitations and future development**

847 While the ELMv1-CNP simulations presented here show that the model is capable of
848 representing contemporary C, N and P stocks and fluxes and capturing the observed
849 ecosystem responses to changes in atmospheric CO_2, the current configuration does have
850 limitations.

851 While the model represents disturbances such as fire and the interactions between
852 disturbances and nutrient cycle dynamics, these interactions and how they affect carbon
853 cycle processes have not been well constrained with observational data. There is a growing
854 body of literature investigating the biogeochemical signature of fire. For example, a meta-
855 analysis by Butler et al. (2018) shows that fire led to significantly higher concentration of
856 soil mineral P and lower soil and litter C:P and N:P ratios, therefore decoupling the P cycle
857 from the C and N cycles. We will take advantage of these recent findings to improve model
858 fidelity on this front.

859 Another area that needs to be improved is the treatment of N fixation and how that is
860 linked to P availability. N fixation in ELMv1-CNP is represented as a function of NPP
861 (Cleveland et al., 1999). While providing a reasonable global estimate of N fixation, the
862 approach ignores existing mechanistic understanding of nitrogen fixation processes
863 (Wieder et al., 2015a). Furthermore, several lines of evidence suggest that both symbiotic
864 and free-living N fixation rates depend on the availability of other elements, such as P and
865 molybdenum (Reed et al., 2013; Nasto et al., 2014). N fixation could have important
866 implications for the spatial distribution of N limitation vs P limitation. In the future we plan
867 to have a more mechanistic representation of N fixation in ELM.

868 In ELMv1-CNP, P limitation is represented by downregulating plant growth when P
869 demand is greater than soil P availability. The mechanisms by which P fundamentally limits
870 ecosystem productivity remain uncertain (Jiang et al., 2019). Some studies proposed that
871 there are linear or log-linear relationships between leaf P concentration and
872 photosynthetic parameters, although the relationship has been shown to be weak (Walker
873 et al., 2014). P fertilization experiments in P limited ecosystems do not support this
874 proposed relationship. A P fertilization experiment on highly weathered soils in Australia

showed that although leaf P concentration increased significantly (+50%) compared to unfertilized trees, photosynthetic capacity was unaffected (Crous et al., 2015). Another fertilization experiment in Hawaii showed that the increase of aboveground NPP with P fertilization was caused mainly by increases in LAI instead of photosynthesis per unit leaf area (Herbert and Fownes, 1995). Further laboratory and field experiments are needed to help us better understand and represent the role of P in photosynthesis. Investigating the detailed mechanisms through which leaf P concentration affects photosynthesis is an active field of research (Jiang et al., 2019; Norby et al., 2017; Crous et al., 2015), and representing these relationships in land models remains an outstanding challenge.

Uncertainty also remains regarding the ELMv1-CNP representation of sorption dynamics and biochemical mineralization and their responses to changes in atmospheric CO_2 and climate (Fleischer et al., 2019). Motivated by our previous modeling studies, several recent field studies have started focusing on improving our mechanistic understanding and providing quantitative relationships for modelling these processes (Cabugao et al., 2017; Brenner et al., 2019). A recent study that upscaled site-measurements of potential phosphatase activity to continental Europe using machine learning technique provides a potential pathway toward generating benchmark data for biochemical mineralization on regional to global scale (Sun et al., 2020). ELMv1-CNP is likely underestimating P leaching, in comparison to the estimate of Wang et al. (2018), which could contribute to the underestimate of P uptake and overestimate of land carbon sink. We will further improve the representation of P leaching in ELMv1. There are other mechanisms that could sustain productivity with increasing P limitation but were not considered in ELMv1-CNP, such as flexible stoichiometry and dynamic allocation. These will be investigated further in future versions of E3SM. However, as Fleischer et al. (2019) pointed out, since plant N:P ratios in highly P limited tropical forests are already at the high end of the observed spectrum, the role of stoichiometry plasticity in sustaining tropical productivity could be limited.

While the representation of NSC has helped ELMv1-CNP to capture the interannual variability of atmospheric CO_2 and to generate ecosystem responses to elevated CO_2 consistent with FACE measurements, the sizes and turnover times of NSC pools are not well

constrained. We will synthesize limited measurements on NSC from literature that include observational and experimental data as well as measurements from isotopic studies to better understand the dynamics of the NSC pool and to evaluate and refine its representation in ELM. We also advocate for more measurements on NSC and how they respond to environmental changes in diverse ecosystems to have a more complete understanding and quantification of NSC.

Finally, although models such as ELMv1-CNP and CLM5 perform similarly when evaluated against present-day metrics as gathered in ILAMB, we expect that the differences among models in their representation of observed processes and in their assumptions about how changes in atmospheric composition and climate will impact ecosystem processes will lead to diverging predictions under future climate scenarios. We will explore those differences and their consequences in future work.

5. Conclusions

In this study, we provide an evaluation of ELMv1-CNP using the ILAMB benchmarking system, comparison with CO_2 manipulation experiments, and comparison with other observational and modeling studies. Benchmarking with ILAMB indicates ELMv1-CNP produces realistic estimates of present-day carbon pools and fluxes. Compared to a simulation with optimal P availability, ELMv1-CNP produces better performance, particularly for the metrics that are most relevant to land-atmosphere exchange. Our results from CO_2 manipulation experiments suggest that ELMv1-CNP is able to capture observed responses to elevated CO_2, including those for GPP, NPP, vegetation C, and LAI. Further analysis suggests that the introduction of a non-structural carbon pool in ELMv1-CNP is largely responsible for these improvements. Evaluating global C, N, and P pools and fluxes in the context of literature values suggests that ELMv1-CNP provides a reasonable representation of contemporary global scale C, N and P cycles.

We highlight the data needs for global land model evaluation, particularly the need for more synthesis datasets on nutrient pools and fluxes, as well as observations from manipulation experiments that provide additional benchmark data for nutrient cycle

evaluation. This need is becoming increasingly pressing as more land models are including N and P cycle dynamics and C-N-P interactions. We also identify challenges in constraining P cycle dynamics and point to the need for soil P measurements.

Our simulations suggest, probably not surprisingly, that in general P is the more limiting nutrient in the tropical regions while N is more limiting in the middle to high latitudes. However, our results also suggest widespread N and P colimitation, even in the tropical regions where P limitation is more dominant. Our results show that C sources and sinks are significantly affected by P limitation, as the historical CO_2 fertilization effect was reduced by 20% and C emission due to LULCC was 11% lower when P limitation was considered. We conclude that introduction of P cycle dynamics and C-N-P coupling will likely have substantial consequences for projections of future C uptake.

Formatted: Subscript

Acknowledgement:

This research was supported as part of the Energy Exascale Earth System Model (E3SM) project, funded by the U.S. Department of Energy, Office of Science, Office of Biological and Environmental Research. This research was also supported by the Oak Ridge National Laboratory's (ORNL) Terrestrial Ecosystem Science Focus Area (TES SFA). F. M. Hoffman was supported by the Reducing Uncertainties in Biogeochemical Interactions through Synthesis and Computation Scientific Focus Area (RUBISCO SFA), which is sponsored by the Regional and Global Model Analysis (RGMA) Program in the Climate and Environmental Sciences Division (CESD) of the Office of Biological and Environmental Research (BER) in the U.S. Department of Energy Office of Science. We thank Min Xu for his help in running ILAMB. The E3SM model can be accessed at https://www.osti.gov/doecode/biblio/10475 (doi: 10.11578/E3SM/dc.20180418.36). The input data is available at https://web.lcrc.anl.gov/public/e3sm/inputdata/.
The model outputs used in this study can be downloaded at the website: https://doi.org/10.6084/m9.figshare.12021348.

References:

Ainsworth, E. A. and Long, S. P.: What have we learned from 15 years of free-air CO2 enrichment (FACE)? A meta-analytic review of the responses of photosynthesis, canopy properties and plant production to rising CO2, New phytologist, 165, 351-372, 2005.
Aragão, L., Malhi, Y., Metcalfe, D., Silva-Espejo, J., Jimenez, E., Navarrete, D., Almeida, S., Costa, A., Salinas, N., and Phillips, O.: Above-and below-ground net primary productivity across ten Amazonian forests on contrasting soils, Biogeosciences, 6, 2759-2778, 2009.

969 Arora, V. K., Boer, G. J., Friedlingstein, P., Eby, M., Jones, C. D., Christian, J. R., Bonan, G.,
970 Bopp, L., Brovkin, V., and Cadule, P.: Carbon–concentration and carbon–climate feedbacks in
971 CMIP5 Earth system models, Journal of Climate, 26, 5289-5314, 2013.
972 Arora, V. K., Katavouta, A., Williams, R. G., Jones, C. D., Brovkin, V., Friedlingstein, P.,
973 Schwinger, J., Bopp, L., Boucher, O., and Cadule, P.: Carbon–concentration and carbon–climate
974 feedbacks in CMIP6 models and their comparison to CMIP5 models, Biogeosciences, 17, 4173-
975 4222, 2020.
976 Avitabile, V., Herold, M., Heuvelink, G. B., Lewis, S. L., Phillips, O. L., Asner, G. P., Armston,
977 J., Ashton, P. S., Banin, L., and Bayol, N.: An integrated pan-tropical biomass map using
978 multiple reference datasets, Global change biology, 22, 1406-1420, 2016.
979 Baig, S., Medlyn, B. E., Mercado, L. M., and Zaehle, S.: Does the growth response of woody
980 plants to elevated CO 2 increase with temperature? A model-oriented meta-analysis, Global
981 change biology, 21, 4303-4319, 2015.
982 Barron, A. R., Wurzburger, N., Bellenger, J. P., Wright, S. J., Kraepiel, A. M., and Hedin, L. O.:
983 Molybdenum limitation of asymbiotic nitrogen fixation in tropical forest soils, Nature
984 Geoscience, 2, 42-45, 2008.
985 Batjes, N. H.: Total carbon and nitrogen in the soils of the world, European journal of soil
986 science, 65, 10-21, 2014.
987 Beer, C., Reichstein, M., Tomelleri, E., Ciais, P., Jung, M., Carvalhais, N., Rödenbeck, C.,
988 Arain, M. A., Baldocchi, D., and Bonan, G. B.: Terrestrial gross carbon dioxide uptake: global
989 distribution and covariation with climate, Science, 329, 834-838, 2010.
990 Bonan, G. B., Lombardozzi, D. L., Wieder, W. R., Oleson, K. W., Lawrence, D. M., Hoffman, F.
991 M., and Collier, N.: Model structure and climate data uncertainty in historical simulations of the
992 terrestrial carbon cycle (1850–2014), Global Biogeochemical Cycles, 33, 1310-1326, 2019.
993 Bonan, G. B., Lawrence, P. J., Oleson, K. W., Levis, S., Jung, M., Reichstein, M., Lawrence, D.
994 M., and Swenson, S. C.: Improving canopy processes in the Community Land Model version 4
995 (CLM4) using global flux fields empirically inferred from FLUXNET data, Journal of
996 Geophysical Research: Biogeosciences, 116, 2011.
997 Brenner, J., Porter, W., Phillips, J. R., Childs, J., Yang, X., and Mayes, M. A.: Phosphorus
998 sorption on tropical soils with relevance to Earth system model needs, Soil research, 57, 17-27,
999 2019.
1000 Burrows, S., Maltrud, M., Yang, X., Zhu, Q., Jeffery, N., Shi, X., Ricciuto, D., Wang, S., Bisht,
1001 G., and Tang, J.: The DOE E3SM v1. 1 Biogeochemistry Configuration: Description and
1002 Simulated Ecosystem-Climate Responses to Historical Changes in Forcing, Journal of Advances
1003 in Modeling Earth Systems, 12, e2019MS001766, 2020.
1004 Butler, O. M., Elser, J. J., Lewis, T., Mackey, B., and Chen, C.: The phosphorus-rich signature of
1005 fire in the soil–plant system: a global meta-analysis, Ecology letters, 21, 335-344, 2018.
1006 Cabugao, K. G., Timm, C. M., Carrell, A. A., Childs, J., Lu, T.-Y. S., Pelletier, D. A., Weston,
1007 D. J., and Norby, R. J.: Root and rhizosphere bacterial phosphatase activity varies with tree
1008 species and soil phosphorus availability in Puerto Rico tropical forest, Frontiers in plant science,
1009 8, 1834, 2017.
1010 Campbell, J., Berry, J., Seibt, U., Smith, S. J., Montzka, S., Launois, T., Belviso, S., Bopp, L.,
1011 and Laine, M.: Large historical growth in global terrestrial gross primary production, Nature,
1012 544, 84-87, 2017.

1013 Cleveland, C., Townsend, A., Schimel, D., Fisher, H., Howarth, R., Hedin, L., Perakis, S., Latty,
1014 E., Von Fischer, J., and Elseroad, A.: Global patterns of terrestrial biological nitrogen (N2)
1015 fixation in natural ecosystems, Global Biogeochemical Cycles, 13, 623-645, 1999.
1016 Collier, N., Hoffman, F. M., Lawrence, D. M., Keppel-Aleks, G., Koven, C. D., Riley, W. J.,
1017 Mu, M., and Randerson, J. T.: The International Land Model Benchmarking (ILAMB) system:
1018 design, theory, and implementation, Journal of Advances in Modeling Earth Systems, 10, 2731-
1019 2754, 2018.
1020 Crews, T. E., Farrington, H., and Vitousek, P. M.: Changes in asymbiotic, heterotrophic nitrogen
1021 fixation on leaf litter of Metrosideros polymorpha with long-term ecosystem development in
1022 Hawaii, Ecosystems, 3, 386-395, 2000.
1023 Crous, K. Y., Osvaldsson, A., and Ellsworth, D. S.: Is phosphorus limiting in a mature
1024 Eucalyptus woodland? Phosphorus fertilisation stimulates stem growth, Plant and soil, 391, 293-
1025 305, 2015.
1026 Davies-Barnard, T. and Friedlingstein, P.: The Global Distribution of Biological Nitrogen
1027 Fixation in Terrestrial Natural Ecosystems, Global Biogeochemical Cycles, 34,
1028 e2019GB006387, 10.1029/2019gb006387, 2020.
1029 Davies-Barnard, T., Meyerholt, J., Zaehle, S., Friedlingstein, P., Brovkin, V., Fan, Y., Fisher, R.
1030 A., Jones, C. D., Lee, H., and Peano, D.: Nitrogen cycling in CMIP6 land surface models:
1031 Progress and limitations, Biogeosciences Discussions, 2020.
1032 DeFries, R., Field, C., Fung, I., Collatz, G., and Bounoua, L.: Combining satellite data and
1033 biogeochemical models to estimate global effects of human-induced land cover change on
1034 carbon emissions and primary productivity, Global biogeochemical cycles, 13, 803-815, 1999.
1035 Du, E., Terrer, C., Pellegrini, A. F., Ahlström, A., van Lissa, C. J., Zhao, X., Xia, N., Wu, X.,
1036 and Jackson, R. B.: Global patterns of terrestrial nitrogen and phosphorus limitation, Nature
1037 Geoscience, 13, 221-226, 2020.
1038 Duarte, H. F., Raczka, B. M., Ricciuto, D. M., Lin, J. C., Koven, C. D., Thornton, P. E.,
1039 Bowling, D. R., Lai, C.-T., Bible, K. J., and Ehleringer, J. R.: Evaluating the Community Land
1040 Model (CLM4. 5) at a coniferous forest site in northwestern United States using flux and carbon-
1041 isotope measurements, Biogeosciences (Online), 14, 2017.
1042 Edwards, E., McCaffery, S., and Evans, J.: Phosphorus availability and elevated CO2 affect
1043 biological nitrogen fixation and nutrient fluxes in a clover dominated sward, New Phytologist,
1044 169, 157-167, 2006.
1045 Ehlers, I., Augusti, A., Betson, T. R., Nilsson, M. B., Marshall, J. D., and Schleucher, J.:
1046 Detecting long-term metabolic shifts using isotopomers: CO2-driven suppression of
1047 photorespiration in C3 plants over the 20th century, Proceedings of the National Academy of
1048 Sciences, 112, 15585-15590, 2015.
1049 Ellsworth, D. S., Anderson, I. C., Crous, K. Y., Cooke, J., Drake, J. E., Gherlenda, A. N.,
1050 Gimeno, T. E., Macdonald, C. A., Medlyn, B. E., and Powell, J. R.: Elevated CO 2 does not
1051 increase eucalypt forest productivity on a low-phosphorus soil, Nature Climate Change, 7, 279-
1052 282, 2017.
1053 Elser, J. J., Bracken, M. E. S., Cleland, E. E., Gruner, D. S., Harpole, W. S., Hillebrand, H.,
1054 Ngai, J. T., Seabloom, E. W., Shurin, J. B., and Smith, J. E.: Global analysis of nitrogen and
1055 phosphorus limitation of primary producers in freshwater, marine and terrestrial ecosystems,
1056 Ecology Letters, 10, 1135-1142, 10.1111/j.1461-0248.2007.01113.x, 2007.

1057 Erb, K.-H., Kastner, T., Plutzar, C., Bais, A. L. S., Carvalhais, N., Fetzel, T., Gingrich, S.,
1058 Haberl, H., Lauk, C., and Niedertscheider, M.: Unexpectedly large impact of forest management
1059 and grazing on global vegetation biomass, Nature, 553, 73-76, 2018.
1060 Finzi, A. C., Norby, R. J., Calfapietra, C., Gallet-Budynek, A., Gielen, B., Holmes, W. E.,
1061 Hoosbeek, M. R., Iversen, C. M., Jackson, R. B., and Kubiske, M. E.: Increases in nitrogen
1062 uptake rather than nitrogen-use efficiency support higher rates of temperate forest productivity
1063 under elevated CO2, Proceedings of the National Academy of Sciences, 104, 14014-14019,
1064 2007.
1065 Fleischer, K., Rammig, A., De Kauwe, M. G., Walker, A. P., Domingues, T. F., Fuchslueger, L.,
1066 Garcia, S., Goll, D. S., Grandis, A., and Jiang, M.: Amazon forest response to CO 2 fertilization
1067 dependent on plant phosphorus acquisition, Nature Geoscience, 12, 736-741, 2019.
1068 Friedlingstein, P., Jones, M., O'Sullivan, M., Andrew, R., Hauck, J., Peters, G., Peters, W.,
1069 Pongratz, J., Sitch, S., and Le Quéré, C.: Global carbon budget 2019, Earth System Science Data,
1070 11, 1783-1838, 2019.
1071 Gerber, S., Hedin, L. O., Oppenheimer, M., Pacala, S. W., and Shevliakova, E.: Nitrogen cycling
1072 and feedbacks in a global dynamic land model, Global Biogeochemical Cycles, 24, GB1001,
1073 10.1029/2008gb003336, 2010.
1074 Ghimire, B., Riley, W. J., Koven, C. D., Mu, M., and Randerson, J. T.: Representing leaf and
1075 root physiological traits in CLM improves global carbon and nitrogen cycling predictions,
1076 Journal of Advances in Modeling Earth Systems, 8, 598-613, 2016.
1077 Goll, D., Winkler, A., Raddatz, T., Dong, N., Prentice, I., Ciais, P., and Brovkin, V.: Carbon–
1078 nitrogen interactions in idealized simulations with JSBACH (version 3.10), Geosci. Model Dev.,
1079 10, 2009–2030, 2017a.
1080 Goll, D., Brovkin, V., Parida, B., Reick, C., Kattge, J., Reich, P., van Bodegom, P., and
1081 Niinemets, U.: Nutrient limitation reduces land carbon uptake in simulations with a model of
1082 combined carbon, nitrogen and phosphorus cycling, Biogeosciences, 9, 3547-3569, 2012.
1083 Goll, D., Vuichard, N., Maignan, F., Jornet-Puig, A., Sardans, J., Violette, A., Peng, S., Sun, Y.,
1084 Kvakic, M., and Guimberteau, M.: A representation of the phosphorus cycle for ORCHIDEE
1085 (revision 4520), 2017b.
1086 Haverd, V., Smith, B., Canadell, J. G., Cuntz, M., Mikaloff-Fletcher, S., Farquhar, G.,
1087 Woodgate, W., Briggs, P. R., and Trudinger, C. M.: Higher than expected CO2 fertilization
1088 inferred from leaf to global observations, Global change biology, 26, 2390-2402, 2020.
1089 Herbert, D. A. and Fownes, J. H.: Phosphorus limitation of forest leaf area and net primary
1090 production on a highly weathered soil, Biogeochemistry, 29, 223-235, 1995.
1091 Herbert, D. A., Williams, M., and Rastetter, E. B.: A model analysis of N and P limitation on
1092 carbon accumulation in Amazonian secondary forest after alternate land-use abandonment,
1093 Biogeochemistry, 65, 121-150, 2003.
1094 Hoffman, F., Koven, C., Keppel-Aleks, G., Lawrence, D., Riley, W., Randerson, J., Ahlström,
1095 A., Abramowitz, G., Baldocchi, D., and Best, M.: International land model benchmarking
1096 (ILAMB) 2016 Workshop Report, US Department of Energy, Office of Science, 10, 1330803,
1097 2017.
1098 Hoffman, F. M., Randerson, J. T., Arora, V. K., Bao, Q., Cadule, P., Ji, D., Jones, C. D.,
1099 Kawamiya, M., Khatiwala, S., and Lindsay, K.: Causes and implications of persistent
1100 atmospheric carbon dioxide biases in Earth System Models, Journal of Geophysical Research:
1101 Biogeosciences, 119, 141-162, 2014.

Hou, E., Tan, X., Heenan, M., and Wen, D.: A global dataset of plant available and unavailable phosphorus in natural soils derived by Hedley method, Scientific data, 5, 180166, 2018.
Hou, E., Luo, Y., Kuang, Y., Chen, C., Lu, X., Jiang, L., Luo, X., and Wen, D.: Global meta-analysis shows pervasive phosphorus limitation of aboveground plant production in natural terrestrial ecosystems, Nature Communications, 11, 1-9, 2020.
Houghton, R. A.: The contemporary carbon cycle, Treatise on geochemistry, 8, 473-513, 2003.
Houlton, B. Z., Wang, Y.-P., Vitousek, P. M., and Field, C. B.: A unifying framework for dinitrogen fixation in the terrestrial biosphere, Nature, 454, 327-330, 10.1038/nature07028, 2008.
Huete, A., Didan, K., Miura, T., Rodriguez, E. P., Gao, X., and Ferreira, L. G.: Overview of the radiometric and biophysical performance of the MODIS vegetation indices, Remote sensing of environment, 83, 195-213, 2002.
Hungate, B. A., Dukes, J. S., Shaw, M. R., Luo, Y., and Field, C. B.: Nitrogen and climate change, Science, 302, 1512-1513, 2003.
Hungate, B. A., Stiling, P. D., Dijkstra, P., Johnson, D. W., Ketterer, M. E., Hymus, G. J., Hinkle, C. R., and Drake, B. G.: CO2 elicits long-term decline in nitrogen fixation, Science, 304, 1291, 2004.
Jahnke, R.: The phosphorus cycle, Global Biogeochemical Cycles, 301-315, 1992.
Jiang, M., Caldararu, S., Zaehle, S., Ellsworth, D. S., and Medlyn, B. E.: Towards a more physiological representation of vegetation phosphorus processes in land surface models, New Phytologist, 222, 1223-1229, 2019.
Jobbágy, E. G. and Jackson, R. B.: The vertical distribution of soil organic carbon and its relation to climate and vegetation, Ecological applications, 10, 423-436, 2000.
Joiner, J., Yoshida, Y., Zhang, Y., Duveiller, G., Jung, M., Lyapustin, A., Wang, Y., and Tucker, C. J.: Estimation of terrestrial global gross primary production (GPP) with satellite data-driven models and eddy covariance flux data, Remote Sensing, 10, 1346, 2018.
Jones, C. D., Arora, V., Friedlingstein, P., Bopp, L., Brovkin, V., Dunne, J., Graven, H., Hoffman, F., Ilyina, T., and John, J. G.: C4MIP–The coupled climate–carbon cycle model intercomparison project: Experimental protocol for CMIP6, Geoscientific Model Development, 9, 2853-2880, 2016.
Jung, C.-G., Shin, H.-J., Park, M.-J., Joh, H.-K., and Kim, S.-J.: Evaluation of MODIS Gross Primary Production (GPP) by Comparing with GPP from CO 2 Flux Data Measured in a Mixed Forest Area, Journal of the Korean Society of Agricultural Engineers, 53, 1-8, 2011.
Kobayashi, H. and Dye, D. G.: Atmospheric conditions for monitoring the long-term vegetation dynamics in the Amazon using normalized difference vegetation index, Remote Sensing of Environment, 97, 519-525, 2005.
Köchy, M., Hiederer, R., and Freibauer, A.: Global distribution of soil organic carbon–Part 1: Masses and frequency distributions of SOC stocks for the tropics, permafrost regions, wetlands, and the world, Soil, 1, 351-365, 2015.
Koven, C., Riley, W., Subin, Z., Tang, J., Torn, M., Collins, W., Bonan, G., Lawrence, D., and Swenson, S.: The effect of vertically resolved soil biogeochemistry and alternate soil C and N models on C dynamics of CLM4, Biogeosciences, 10, 7109, 2013.
Lawrence, D. M., Fisher, R. A., Koven, C. D., Oleson, K. W., Swenson, S. C., Bonan, G., Collier, N., Ghimire, B., van Kampenhout, L., and Kennedy, D.: The Community Land Model version 5: Description of new features, benchmarking, and impact of forcing uncertainty, Journal of Advances in Modeling Earth Systems, 2019.

Le Quéré, C., Andrew, R., Canadell, J. G., Sitch, S., Korsbakken, J. I., Peters, G. P., Manning, A. C., Boden, T. A., Tans, P. P., and Houghton, R. A.: Global carbon budget 2016, 2016.
Le Quéré, C., Andrew, R. M., Friedlingstein, P., Sitch, S., Hauck, J., Pongratz, J., Pickers, P. A., Korsbakken, J. I., Peters, G. P., and Canadell, J. G.: Global carbon budget 2018, Earth System Science Data, 10, 2141-2194, 2018.
LeBauer, D. S. and Treseder, K. K.: Nitrogen limitation of net primary productivity in terrestrial ecosystems is globally distributed, Ecology, 89, 371-379, 2008.
Lin, B.-L., Sakoda, A., Shibasaki, R., Goto, N., and Suzuki, M.: Modelling a global biogeochemical nitrogen cycle in terrestrial ecosystems, Ecological Modelling, 135, 89-110, 2000.
Luo, Y., Randerson, J. T., Friedlingstein, P., Hibbard, K., Hoffman, F., Huntzinger, D., Jones, C., Koven, C., Lawrence, D., and Li, D.: A framework for benchmarking land models, 2012.
Mao, J., Ricciuto, D. M., Thornton, P. E., Warren, J. M., King, A. W., Shi, X., Iversen, C. M., and Norby, R. J.: Evaluating the Community Land Model in a pine stand with shading manipulations and 13CO2 labeling, Biogeosciences (Online), 13, 2016.
Marklein, A. R. and Houlton, B. Z.: Nitrogen inputs accelerate phosphorus cycling rates across a wide variety of terrestrial ecosystems, New Phytologist, 193, 696-704, 2012.
Matthews, E.: Global litter production, pools, and turnover times: Estimates from measurement data and regression models, Journal of Geophysical Research: Atmospheres, 102, 18771-18800, 1997.
McGill, W. and Cole, C.: Comparative aspects of cycling of organic C, N, S and P through soil organic matter, Geoderma, 26, 267-286, 1981.
Melillo, J., Steudler, P., Aber, J., Newkirk, K., Lux, H., Bowles, F., Catricala, C., Magill, A., Ahrens, T., and Morrisseau, S.: Soil warming and carbon-cycle feedbacks to the climate system, Science, 298, 2173-2176, 2002.
Metcalfe, D. B., Ricciuto, D., Palmroth, S., Campbell, C., Hurry, V., Mao, J., Keel, S. G., Linder, S., Shi, X., and Näsholm, T.: Informing climate models with rapid chamber measurements of forest carbon uptake, Global change biology, 23, 2130-2139, 2017.
Mitchard, E. T., Feldpausch, T. R., Brienen, R. J., Lopez-Gonzalez, G., Monteagudo, A., Baker, T. R., Lewis, S. L., Lloyd, J., Quesada, C. A., and Gloor, M.: Markedly divergent estimates of A mazon forest carbon density from ground plots and satellites, Global Ecology and Biogeography, 23, 935-946, 2014.
Nakhavali, M., Mercado, L. M., Hartley, I. P., Sitch, S., Cunha, F. V., di Ponzio, R., Lugli, L. F., Quesada, C. A., Andersen, K. M., and Chadburn, S. E.: Representation of phosphorus cycle in Joint UK Land Environment Simulator (vn5. 5_JULES-CNP), Geoscientific Model Development Discussions, 1-24, 2021.
Nasto, M. K., Alvarez-Clare, S., Lekberg, Y., Sullivan, B. W., Townsend, A. R., and Cleveland, C. C.: Interactions among nitrogen fixation and soil phosphorus acquisition strategies in lowland tropical rain forests, Ecology Letters, 17, 1282-1289, 2014.
Norby, R. J., Gu, L., Haworth, I. C., Jensen, A. M., Turner, B. L., Walker, A. P., Warren, J. M., Weston, D. J., Xu, C., and Winter, K.: Informing models through empirical relationships between foliar phosphorus, nitrogen and photosynthesis across diverse woody species in tropical forests of Panama, New Phytologist, 215, 1425-1437, 2017.
Olander, L. P. and Vitousek, P. M.: Regulation of soil phosphatase and chitinase activityby N and P availability, Biogeochemistry, 49, 175-191, 2000.

Oleson, K., Lawrence, D., Bonan, G., Drewniak, B., Huang, M., Koven, C., Levis, S., Li, F., Riley, W., and Subin, Z.: Technical Description of version 4.5 of the Community Land Model (CLM)(NCAR Technical Note No. NCAR/TN-503+ STR). Citeseer, National Center for Atmospheric Research, PO Box, 3000, 2013.
Pan, Y., Birdsey, R. A., Fang, J., Houghton, R., Kauppi, P. E., Kurz, W. A., Phillips, O. L., Shvidenko, A., Lewis, S. L., and Canadell, J. G.: A large and persistent carbon sink in the world,Äôs forests, Science, 333, 988-993, 2011.
Post, W. M., Pastor, J., Zinke, P. J., and Stangenberger, A. G.: Global patterns of soil nitrogen storage, Nature, 317, 613-616, 1985.
Raczka, B., Duarte, H. F., Koven, C. D., Ricciuto, D., Thornton, P. E., Lin, J. C., and Bowling, D. R.: An observational constraint on stomatal function in forests: evaluating coupled carbon and water vapor exchange with carbon isotopes in the Community Land Model (CLM4. 5), Biogeosciences, 13, 5183-5204, 2016.
Reed, S. C., Cleveland, C. C., and Townsend, A. R.: Relationships among phosphorus, molybdenum and free-living nitrogen fixation in tropical rain forests: results from observational and experimental analyses, Biogeochemistry, 1-13, 2013.
Reed, S. C., Yang, X., and Thornton, P. E.: Incorporating phosphorus cycling into global modeling efforts: a worthwhile, tractable endeavor, New Phytologist, 208, 324-329, 2015.
Santoro, M., Beaudoin, A., Beer, C., Cartus, O., Fransson, J. E., Hall, R. J., Pathe, C., Schmullius, C., Schepaschenko, D., and Shvidenko, A.: Forest growing stock volume of the northern hemisphere: Spatially explicit estimates for 2010 derived from Envisat ASAR, Remote Sensing of Environment, 168, 316-334, 2015.
Sellar, A. A., Jones, C. G., Mulcahy, J., Tang, Y., Yool, A., Wiltshire, A., O'connor, F. M., Stringer, M., Hill, R., and Palmieri, J.: UKESM1: Description and evaluation of the UK Earth System Model, Journal of Advances in Modeling Earth Systems, 2019.
Shabanov, N. V., Huang, D., Yang, W., Tan, B., Knyazikhin, Y., Myneni, R. B., Ahl, D. E., Gower, S. T., Huete, A. R., and Aragão, L. E. O.: Analysis and optimization of the MODIS leaf area index algorithm retrievals over broadleaf forests, IEEE Transactions on Geoscience and Remote Sensing, 43, 1855-1865, 2005.
Smil, V.: P HOSPHORUS IN THE E NVIRONMENT: Natural Flows and Human Interferences, Annual review of energy and the environment, 25, 53-88, 2000.
Smith, B., Warlind, D., Arneth, A., Hickler, T., Leadley, P., Siltberg, J., and Zaehle, S.: Implications of incorporating N cycling and N limitations on primary production in an individual-based dynamic vegetation model, Biogeosciences, 11, 2027-2054, 2014.
Sun, Y., Goll, D. S., Ciais, P., Peng, S., Margalef, O., Asensio, D., Sardans, J., and Peñuelas, J.: Spatial pattern and environmental drivers of acid phosphatase activity in Europe, 2020.
Sun, Y., Goll, D. S., Chang, J., Ciais, P., Guenet, B., Helfenstein, J., Huang, Y., Lauerwald, R., Maignan, F., and Naipal, V.: Global evaluation of the nutrient-enabled version of the land surface model ORCHIDEE-CNP v1. 2 (r5986), Geoscientific Model Development, 14, 1987-2010, 2021.
Sun, Y., Peng, S., Goll, D. S., Ciais, P., Guenet, B., Guimberteau, M., Hinsinger, P., Janssens, I. A., Peñuelas, J., and Piao, S.: Diagnosing phosphorus limitations in natural terrestrial ecosystems in carbon cycle models, Earth's future, 5, 730-749, 2017.
Terrer, C., Jackson, R. B., Prentice, I. C., Keenan, T. F., Kaiser, C., Vicca, S., Fisher, J. B., Reich, P. B., Stocker, B. D., and Hungate, B. A.: Nitrogen and phosphorus constrain the CO 2 fertilization of global plant biomass, Nature Climate Change, 9, 684-689, 2019.

1239 Thornton, P., Doney, S., Lindsay, K., Moore, J., Mahowald, N., Randerson, J., Fung, I.,
1240 Lamarque, J., Feddema, J., and Lee, Y.: Carbon-nitrogen interactions regulate climate-carbon
1241 cycle feedbacks: results from an atmosphere-ocean general circulation model, 2009.
1242 Thornton, P. E., Lamarque, J.-F., Rosenbloom, N. A., and Mahowald, N. M.: Influence of
1243 carbon-nitrogen cycle coupling on land model response to CO2 fertilization and climate
1244 variability, Global Biogeochemical Cycles, 21, GB4018, 10.1029/2006gb002868, 2007.
1245 Thum, T., Caldararu, S., Engel, J., Kern, M., Pallandt, M., Schnur, R., Yu, L., and Zaehle, S.: A
1246 new terrestrial biosphere model with coupled carbon, nitrogen, and phosphorus cycles (QUINCY
1247 v1. 0; revision 1772), Geoscientific Model Development, 12, 4781-4802, 2019.
1248 Todd-Brown, K., Randerson, J., Post, W., Hoffman, F., Tarnocai, C., Schuur, E., and Allison, S.:
1249 Causes of variation in soil carbon simulations from CMIP5 Earth system models and comparison
1250 with observations, Biogeosciences, 10, 1717-1736, 2013.
1251 Treseder, K. K. and Vitousek, P. M.: Effects of soil nutrient availability on investment in
1252 acquisition of N and P in Hawaiian rain forests, Ecology, 82, 946-954, 2001.
1253 Van den Hurk, B., Kim, H., Krinner, G., Seneviratne, S. I., Derksen, C., Oki, T., Douville, H.,
1254 Colin, J., Ducharne, A., and Cheruy, F.: LS3MIP (v1. 0) contribution to CMIP6: the Land
1255 Surface, Snow and Soil moisture Model Intercomparison Project-aims, setup and expected
1256 outcome, Geoscientific Model Development, 9, 2809-2832, 2016.
1257 Vicca, S., Luyssaert, S., Penuelas, J., Campioli, M., Chapin III, F., Ciais, P., Heinemeyer, A.,
1258 Högberg, P., Kutsch, W., and Law, B. E.: Fertile forests produce biomass more efficiently,
1259 Ecology letters, 15, 520-526, 2012.
1260 Vitousek, P. M., Menge, D. N., Reed, S. C., and Cleveland, C. C.: Biological nitrogen fixation:
1261 rates, patterns and ecological controls in terrestrial ecosystems, Philosophical Transactions of the
1262 Royal Society B: Biological Sciences, 368, 20130119, 2013.
1263 Vitousek, P. M., Porder, S., Houlton, B. Z., and Chadwick, O. A.: Terrestrial phosphorus
1264 limitation: mechanisms, implications, and nitrogen-phosphorus interactions, Ecological
1265 applications, 20, 5-15, 2010.
1266 Walker, A. P., Beckerman, A. P., Gu, L., Kattge, J., Cernusak, L. A., Domingues, T. F., Scales,
1267 J. C., Wohlfahrt, G., Wullschleger, S. D., and Woodward, F. I.: The relationship of leaf
1268 photosynthetic traits–Vcmax and Jmax–to leaf nitrogen, leaf phosphorus, and specific leaf area: a
1269 meta-analysis and modeling study, Ecology and evolution, 4, 3218-3235, 2014.
1270 Walker, T. and Syers, J.: The fate of phosphorus during pedogenesis, Geoderma, 15, 1-19, 1976.
1271 Wang, Y., Ciais, P., Goll, D. S., Huang, Y., Luo, Y., Wang, Y.-P., Bloom, A. A., Broquet, G.,
1272 Hartmann, J., and Peng, S.: GOLUM-CNP v1. 0: a data-driven modeling of carbon, nitrogen and
1273 phosphorus cycles in major terrestrial biomes, 2018.
1274 Wang, Y.-P., Law, R. M., and Pak, B.: A global model of carbon, nitrogen and phosphorus
1275 cycles for the terrestrial biosphere, Biogeosciences, 7, 2261-2282, 10.5194/bg-7-2261-2010,
1276 2010.
1277 Wang, Y. P., Houlton, B. Z., and Field, C. B.: A model of biogeochemical cycles of carbon,
1278 nitrogen, and phosphorus including symbiotic nitrogen fixation and phosphatase production,
1279 Global Biogeochemical Cycles, 21, GB1018, 10.1029/2006gb002797, 2007.
1280 Welp, L. R., Keeling, R. F., Meijer, H. A., Bollenbacher, A. F., Piper, S. C., Yoshimura, K.,
1281 Francey, R. J., Allison, C. E., and Wahlen, M.: Interannual variability in the oxygen isotopes of
1282 atmospheric CO 2 driven by El Niño, Nature, 477, 579-582, 2011.

Wieder, W. R., Cleveland, C. C., Lawrence, D. M., and Bonan, G. B.: Effects of model structural uncertainty on carbon cycle projections: biological nitrogen fixation as a case study, Environmental Research Letters, 10, 044016, 2015a.
Wieder, W. R., Cleveland, C. C., Smith, W. K., and Todd-Brown, K.: Future productivity and carbon storage limited by terrestrial nutrient availability, Nature Geoscience, 8, 441, 2015b.
Wieder, W. R., Lawrence, D. M., Fisher, R. A., Bonan, G. B., Cheng, S. J., Goodale, C. L., Grandy, A. S., Koven, C. D., Lombardozzi, D. L., and Oleson, K. W.: Beyond static benchmarking: Using experimental manipulations to evaluate land model assumptions, Global Biogeochemical Cycles, 33, 1289-1309, 2019.
Wright, S. J., Turner, B. L., Yavitt, J. B., Harms, K. E., Kaspari, M., Tanner, E. V., Bujan, J., Griffin, E. A., Mayor, J. R., and Pasquini, S. C.: Plant responses to fertilization experiments in lowland, species-rich, tropical forests, Ecology, 99, 1129-1138, 2018.
Xu, R. I. and Prentice, I. C.: Terrestrial nitrogen cycle simulation with a dynamic global vegetation model, Global Change Biology, 14, 1745-1764, 10.1111/j.1365-2486.2008.01625.x, 2008.
Yang, X. and Post, W.: Phosphorus transformations as a function of pedogenesis: a synthesis of soil phosphorus data using Hedley fractionation method, Biogeosciences, 8, 2907-2916, 2011.
Yang, X., Post, W., Thornton, P., and Jain, A.: The distribution of soil phosphorus for global biogeochemical modeling, Biogeosciences, 10, 2525-2537, 2013.
Yang, X., Thornton, P., Ricciuto, D., and Post, W.: The role of phosphorus dynamics in tropical forests–a modeling study using CLM-CNP, Biogeosciences, 11, 1667-1681, 2014.
Yang, X., Thornton, P. E., Ricciuto, D. M., and Hoffman, F. M.: Phosphorus feedbacks constraining tropical ecosystem responses to changes in atmospheric CO2 and climate, Geophysical Research Letters, 43, 7205-7214, 10.1002/2016GL069241, 2016.
Yang, X., Wittig, V., Jain, A., and Post, W.: Integration of nitrogen cycle dynamics into the Integrated Science Assessment Model for the study of terrestrial ecosystem responses to global change, Global Biogeochemical Cycles, 23, 2009.
Yang, X., Ricciuto, D. M., Thornton, P. E., Shi, X., Xu, M., Hoffman, F., and Norby, R. J.: The effects of phosphorus cycle dynamics on carbon sources and sinks in the Amazon region: a modeling study using ELM v1, Journal of Geophysical Research: Biogeosciences, 2019.
Zaehle, S., Friend, A., Friedlingstein, P., Dentener, F., Peylin, P., and Schulz, M.: Carbon and nitrogen cycle dynamics in the O-CN land surface model: 2. Role of the nitrogen cycle in the historical terrestrial carbon balance, Global Biogeochemical Cycles, 24, 2010.
Zhang, Q., Wang, Y.-P., Matear, R., Pitman, A., and Dai, Y.: Nitrogen and phosphorous limitations significantly reduce future allowable CO2 emissions, Geophysical Research Letters, 41, 632-637, 2014.
Zhu, Q., Riley, W. J., Tang, J., Collier, N., Hoffman, F. M., Yang, X., and Bisht, G.: Representing nitrogen, phosphorus, and carbon interactions in the E3SM land model: Development and global benchmarking, Journal of Advances in Modeling Earth Systems, 11, 2238-2258, 2019.

1327
1328
1329
1330
1331
1332
1333
1334
1335
1336
1337
1338
1339

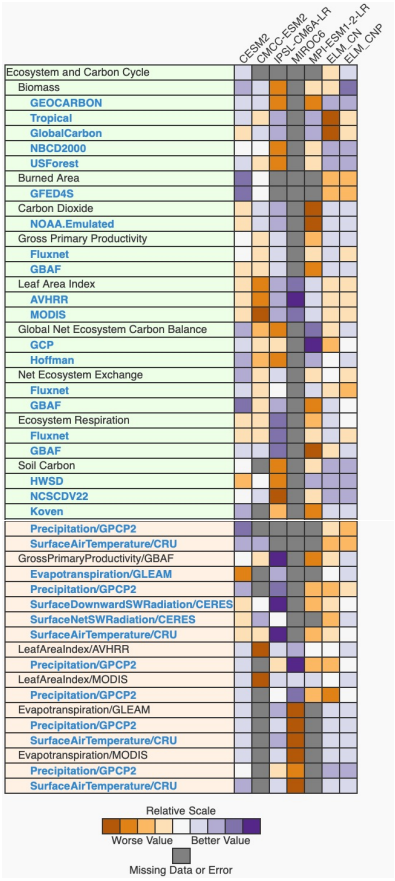

Figure 1: ILAMB carbon cycle scores for ELMv1-CNP and ELM-CN and a few land models in CMIP6. Shown here is the relative score, indicating the performance of each model relative to other models. References for benchmarking data for each variable are provided in Table S4. The datasets that are in green boxes are either carbon pools or fluxes while the datasets in orange boxes are relationships between carbon pools/fluxes and environmental variables such as precipitation or temperature. Outputs for other land models are from the LS3MIP offline simulations archive in CMIP6. These simulations were performed using the same resolution and forcing data as this study. CLM4.5 is the land model in CMCC-ESM2. CLM5 is the land model for

CESM2. OCHIDEE is the land model for IPSL. JSBACH is the land model for MPI-ESM1.2. VISIT is the land model for MIROC6.

Deleted: A

Deleted: P

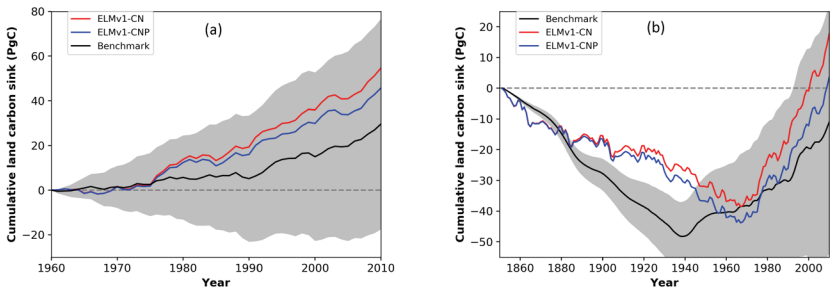

Figure 2: ELMv1-CNP and ELMv1-CN simulated global land carbon accumulation for the time period (a) 1960-2010 and (b) and 1850-2010. Benchmark data (black lines with uncertainty estimate in grey) are from (a) Global carbon project (Le Quere et al., 2016) and (b) Hoffman et al. (2014).

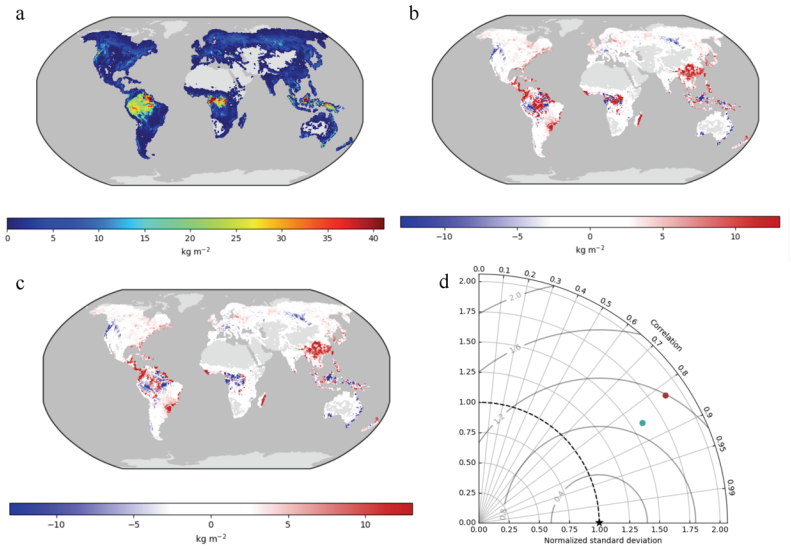

Figure 3: Global pattern of simulated biomass: (a) benchmark data, (b) ELMv1-CN bias (c) ELMv1-CNP bias and (d) spatial Taylor diagram for model-benchmark comparison (red dot is for ELMv1-CN and blue dot is for ELMv1-CNP). Benchmark data here is from the GEOCARBON product (Saatchi et al.,2011).

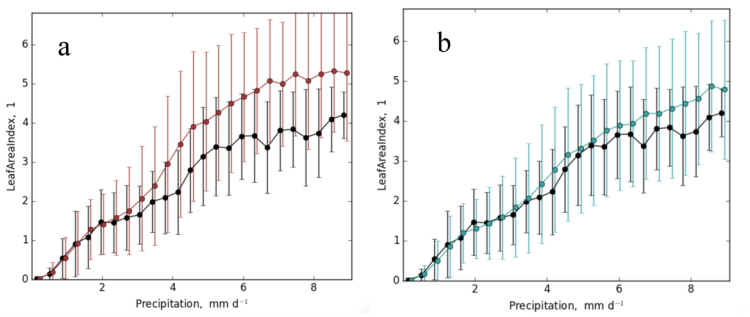

Figure 4: ILAMB relationship plot between LAI and climatological annual precipitation and (a) ELMv1-CN (b) ELMv1-CNP. Black line is the observationally derived relationship. Error bars indicate one standard derivation of LAI for all grid cells within the precipitation bin. Observed LAI is from MODIS LAI product.

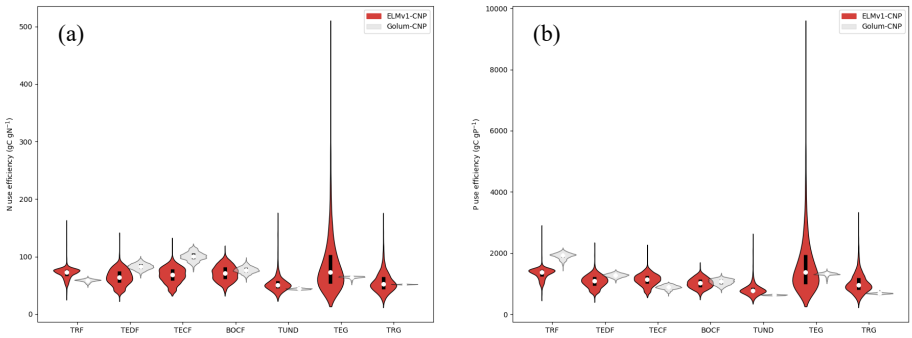

Figure 5: Violin plots of (a) nitrogen use efficiency (NUE) and (b) phosphorus use efficiency (PUE) from ELMv1-CNP and GOLUM-CNP for seven biomes: tropical rainforest (TRF), temperate deciduous forest (TEDF), temperate coniferous forest (TECF), boreal coniferous forest (BOCF), temperate grassland (TEG) and tropical grassland (TRG). Plots show the medians of all grid cells in each biome (open circles) and the probability density distribution (balloons).

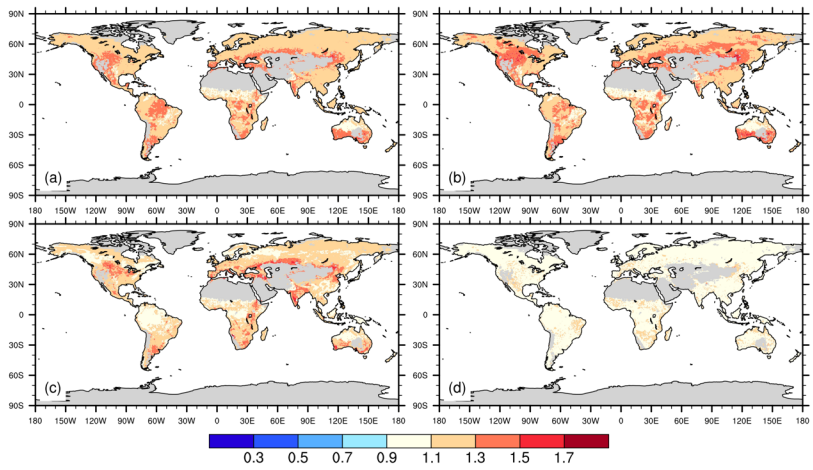

Figure 6: Spatial distribution of the effect size of CO_2 enrichment on (a) GPP (b) NPP (c) Vegetation carbon (d) LAI. Effect sizes were calculated for each grid cell as the mean annual values of GPP, NPP, vegetation carbon and LAI from CO_2 enrichment simulation divided those from the control simulations between 2001-2010.

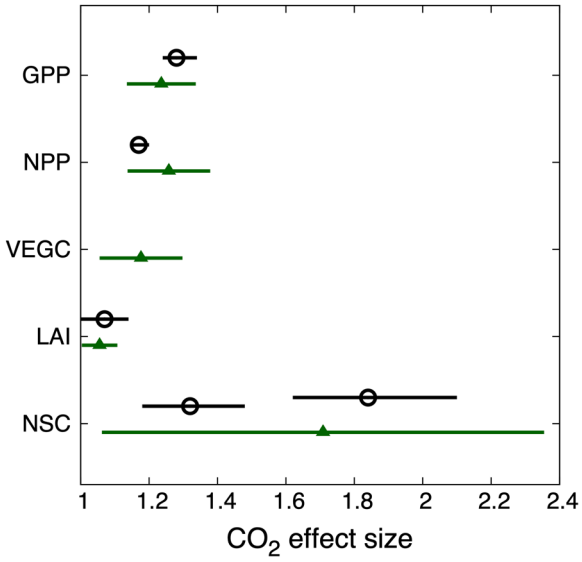

Figure 7: Observed (open circles) and simulated (green triangles) effect size of CO_2 enrichment on GPP, NPP, LAI, vegetation carbon and non-structural carbon. Observations show the mean (±95% confidence interval; Ainsworth and Long, 2005). There are two observations of NSC shown here, one is for sugar with a mean value of 1.3 and the other is for starch with a mean value of 1.8, while model conceptualization of NSC includes both sugar and starch. Simulated responses show the global mean effect sizes (± stand derivation; calculated to provide an estimate of spatial variation).

Deleted: solid circles

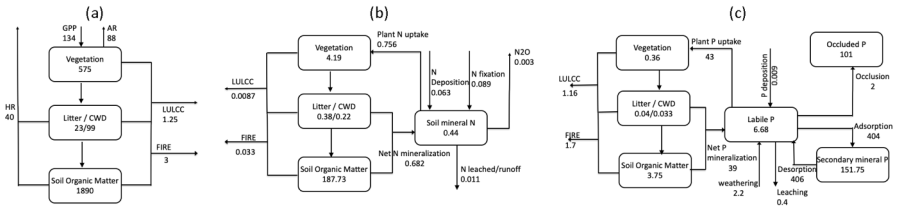

Figure 8: (left) terrestrial C cycle, (middle) N cycle, and (right) P cycle as simulated by ELMv1-CNP, shown here are mean values between 2001-2010. Vegetation and soil C, N and P pools are in units of Pg C, Pg N and Pg P, respectively. C and N fluxes are given in Pg C yr^{-1} and Pg N yr^{-1}, and P fluxes are given in Tg P yr^{-1}. AR stands for autotrophic respiration and HR stands for heterotrophic respiration.

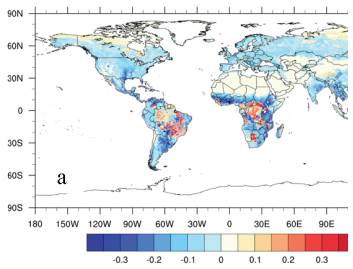

Deleted:

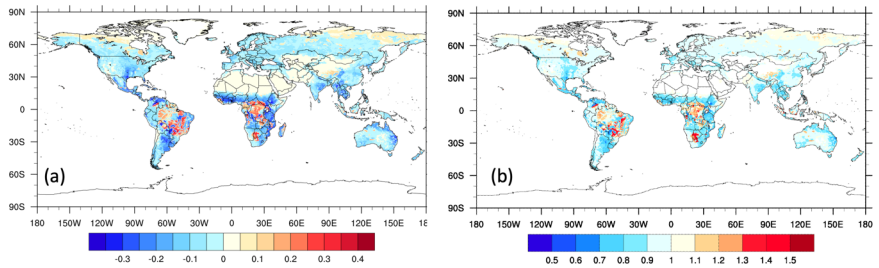

Figure 9: (a) Spatial variation of the extent of nutrient limitation on plant growth. Regions with a negative value are more limited by N, while regions with a positive value are more limited by P. Larger absolute values are associated with stronger limitation. Values plotted are the proportion by which plant growth is reduced due to N limitation or P limitation: 1-f_P when f_P <f_N and f_N-1 when f_N <f_P, where f_P is the limitation factor on plant growth considering P supply and demand, while f_N is the limitation factor on plant growth considering N supply and demand (Yang *et al.*, 2014). (b) Spatial variation of the ratios between P limitation and N limitation indicating the degree of co-limitation. Values plotted are the ratios between f_N and f_P: f_N/f_P. Regions with values less than 1 indicate more N limitation and regions with values greater than 1 are more limited by P. Values close to 1 indicate NP co-limitation. Definition of colimitation is subjective here, but difference of 10% or less between the values for f_N and f_P would lead to a range of about 0.9 to 1.1 in the plotted ratio.

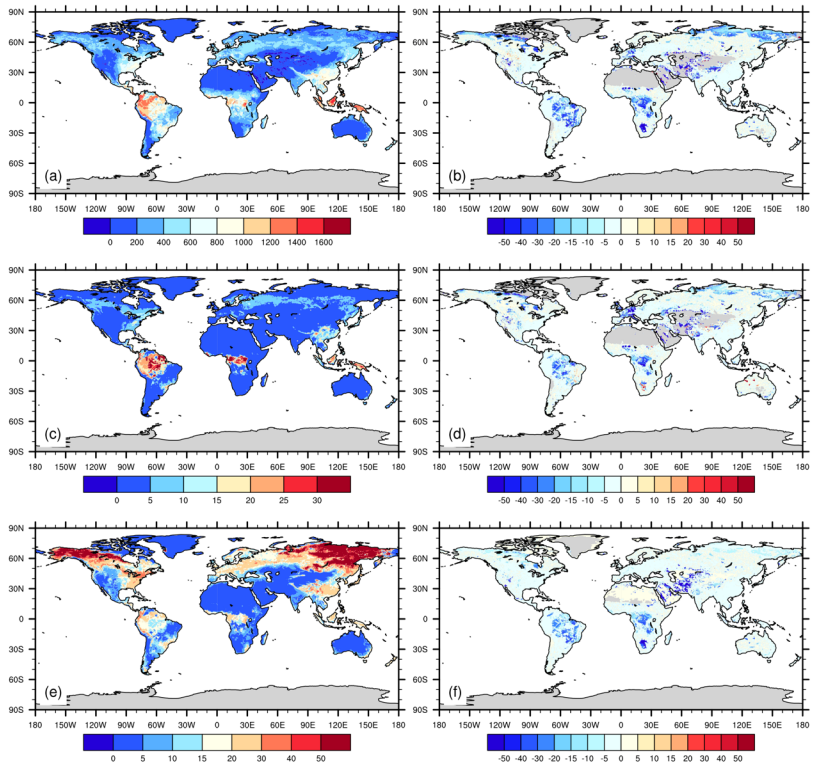

Fig. 10: Average estimates of (a) net primary productivity (g C m^{-2} yr^{-1}) (c) vegetation carbon (kg C m^{-2}) and (e) soil organic carbon (kg C m^{-2}) for the years 2001-2010 and the effects of phosphorus dynamics (expressed as percentage deviation between CNP and CN configurations, unitless) on (b) net primary productivity (d) vegetation carbon (f) soil carbon as estimated by ELMv1.

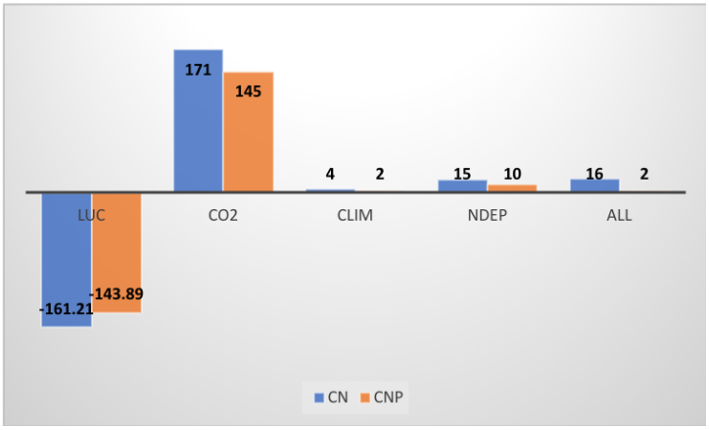

Fig. 11: Cumulative global carbon storage (Pg C) from 1850 to 2010 from ELMv1-CN and ELMv1-CNP simulations with changes in land use and land cover change (LUC), atmospheric CO_2 (CO_2), climate (CLIM), N deposition (NDEP), and all factor combined (ALL). These are calculated as the accumulation of NEE between 1850 and 2010 for the historical transient model simulations listed in Table 1.

Deleted: 0

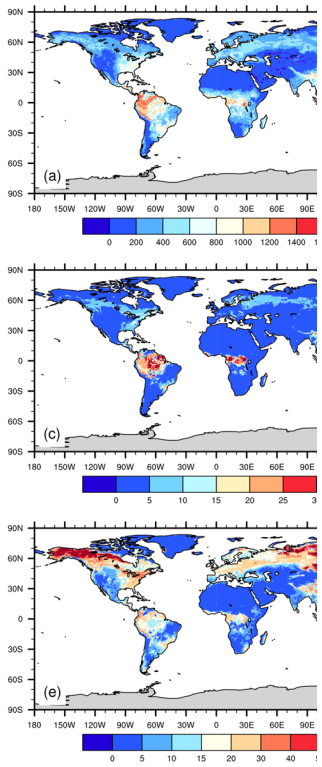

Deleted: ¶

Fig. 11: Average estimates and effects of phosphorus dynamics on (a,b) net primary productivity, (c,d) vegetation carbon and (e,f) soil organic carbon for the years 2001-2010, as estimated by ELM v1. The effects of P dynamics are expressed as percentage deviation between CNP and CN configurations¶

Deleted: ¶

Table 1: Summary of model simulations

Experiment	P coupling	CO_2 forcing	LULCC	Climate forcing	N depos
Ctrl_CN	off	1850	1850	steady state[a]	1850
Ctrl_CNP	on	1850	1850	steady state[a]	1850
Hist_CN_CO_2	off	transient	1850	steady state[a]	1850
Hist_CNP_CO_2	on	transient	1850	steady state[a]	1850
Hist_CN_LUC	off	1850	transient	steady state[a]	1850
Hist_CNP_LUC	on	1850	transient	steady state[a]	1850
Hist_CN_climate	off	1850	1850	transient[b]	1850
Hist_CNP_ climate	on	1850	1850	transient[b]	1850
Hist_CN_NDep	off	1850	1850	steady state[a]	transient
Hist_CNP_Ndep	on	1850	1850	steady state[a]	transient
Hist_CN_all	off	Transient	A d	transient[b]	transient
Hist_CNP_all	on	transient	transient	transient[b]	transient
FACE_CO_2	on	+200ppm (1991-2010)	transient	transient[b]	transient

a Cycling of 20-year time series of GSWP3 reanalysis product (1901-1920)
b Historical time series of GSWP3 reanalysis product (1901-2010)

Formatted: Subscript

Deleted: i

1516 Table 2: Comparison of ELMv1-CNP Simulated Mean Global Stocks and Fluxes of C, N and P
1517 between 2001 and 2010 to Observation-based Estimates

	ELMv1-CNP	Observation-based Estimates		
			Source	Methodology
GPP (Pg C yr^{-1})	134.15	123±8	Beer et al., 2010	Using eddy covariance flux data and various diagnostic models
		150-175	Welp et al., 2011	Based on oxygen isotopes of atmospheric CO_2
		119±6	Jung et al., 2011	upscaled FLUXNET observations to the global scale using the machine learning technique, model tree ensembles (MTE).
		121.60 - 129.42	Zhang et al., 2017	Light use efficiency theory, MODIS satellite data and climate data
		140	Joiner et al., 2018	Satellite Data-Driven Models and Eddy Covariance Flux Data
NPP (Pg C yr^{-1})	46.09	55±11	Turner et al., 2006	MODIS products
		33-49	Smith et al., 2016	MODIS NPP algorithm driven by long-term Global Inventory Modeling and Mapping Studies (GIMMS) FPAR and LAI data
Vegetation C (Pg C)	575.45	550±100	Houghton, 2003	Literature synthesis
		560±94	Defries et al., 1999	
Soil carbon (Pg C)	1890.78	1750±250	Houghton, 2003	Literature synthesis
		2344	Jobbagy and Jackson, 2000	based on >2700 soil profiles in three global databases supplemented with data for climate, vegetation, and land use.
		3000	Kochy et al., 2015	Based on the Harmonized World Soil Database(HWSD), but with more detailed estimates for permafrost and tropical wetland soil carbon
		2376–2456	Batjes, 2014	Top 2m. Based on 4353 soil profiles distributed globally and the FAO Soil Map of the World.
Top 1m soil carbon (Pg C)	1134.41	1462-1548	Batjes, 2014	Based on 4353 soil profiles distributed globally and the FAO Soil Map of the World.
		1325	Kochy et al., 2015	Based on the Harmonized World Soil Database(HWSD), but with more detailed estimates for permafrost and tropical wetland soil carbon
		1502	Jobbagy and Jackson, 2000	based on >2700 soil profiles in three global databases supplemented with

				data for climate, vegetation, and land use.
Soil organic N (Pg N)	188.79	95	Post et al. 1985	Based on 3100 soil profiles and a global map of Holdridge life zones
		133-140	Batjes et al., 2014	Top 1m. Based on 4353 soil profiles distributed globally and the FAO Soil Map of the World
N fixation (Tg N yr^{-1})	89	40-100	Vitousek et al., 2013	Estimates for Pre-industrial. Combining information on N fluxes with ^{15}N relative abundance data for terrestrial ecosystems
		52-130	Davies-Barnard and Friedlingstein (2020)	Based on a comprehensive meta-analysis of field measurements
N uptake (Tg N yr^{-1})	760	570	Wang et al., 2018	Data-driven estimates. Observations include observed stoichiometric ratios, N and P external input fluxes, and the fraction of gaseous losses of N to total (gaseous and leaching) losses of N from a global data set of ^{15}N measurements in soils
N Leaching (Tg N yr^{-1})	12	38	Wang et al., 2018	Data-driven estimates. See above
		28	Mayorga et al., 2010	based on a mass-balance approach for the land surface (watershed) and river system for year 2000
P uptake (Tg P yr^{-1})	43	26	Wang et al., 2018	Data-driven estimates. See above
P leaching (Tg P yr^{-1})	0.46	2.6	Wang et al., 2018	Data-driven estimates. See above
P occlusion (Tg P yr^{-1})	1.85	1.3	Wang et al., 2018	Data-driven estimates. See above

Supporting Information for

Global evaluation of ELMv1-CNP and the role of the phosphorus cycle in the historical terrestrial carbon balance

Xiaojuan Yang[1*], Peter Thornton[1], Daniel Ricciuto[1], Yilong Wang[2,3], Forrest Hoffman[4]

[1]Environmental Sciences Division, Oak Ridge National Lab, Oak Ridge, TN 37831

[2]Key Laboratory of Land Surface Pattern and Simulation, Institute of Geographic Sciences and Natural Resources Research, Chinese Academy of Sciences, Beijing, China

[3]Laboratoire des Sciences du Climat et de l'Environnement, CEA-CNRS-UVSQ- Université Paris Saclay, 91191, Gif-sur-Yvette CEDEX, France

[4]Computational Sciences & Engineering Division, Oak Ridge National Lab, Oak Ridge, TN 37831

Contents of this file

Text S1

Figures S1 to S9

Tables S1 to S4

Introduction

This supporting information provides supplementary text, figures and tables for the main article.

Text S1: Additional description of the representation of Non-structural (NSC) pool in ELMv1-CNP

In the current model configuration, there are no direct feedbacks of the non-structural carbon pool on plant activities. When soil nutrient supply is high, allocation to new NSC decreases and allocation to biomass construction increases, and the size of the NSC pool declines; however, existing NSC turns over to the atmosphere and is not utilized by plants.

The respiration from the NSC pool R_{NSC} is calculated using the following equation:

$$R_{NSC} = br_{cpool} * C_{NSC} * Q_{10}^{(Tair-298.15)/10}$$

Where br_{cpool} is the respiration base rate at 25°C, which is set to 10^{-9} gC m^{-2} s^{-1}. This is equivalent to roughly a 3-year turnover time for the NSC pool C_{NSC}, which is broadly consistent with observations that indicate a range of values across plant components and NSC forms with a weighted mean of 2-3 years (Richardson et al., 2015). The Q_{10} parameter, which has a value of 1.5 in these simulations, controls the strength of the temperature response. T_{air} is the 2-meter air temperature (K).

Nutrients are allocated from the non-structural pools using the following equation:

$$N_{alloc} = \frac{N_{demand}}{max\left(\frac{N_{NS,max}}{N_{NS}}, 1\right)}$$

Where N_{demand} is the amount of nutrient (nitrogen or phosphorus) required to allocate all NPP during a model timestep to plant structural pools given the stoichiometry. N_{NS} is the size of the non-structural nutrient pool, and $N_{NS,max}$ is the size of the pool above which there is no nutrient limitation.

$$N_{NS,max} = Nstor * NPP_{N,anual}$$

$NPP_{N,annual}$ is the previous year's total of annual net primary productivity for the nutrient of interest. The parameter *Nstor* is set to 3 for these simulations. Therefore, nutrient limitation only affects allocation when there are less than 3 years of non-structural nutrient storage. This is consistent with the average age of NSC found by (Richardson et al., 2015), though that analysis found a 2-pool NSC model may have more predictive skill, which we will consider implementing in future work.

These computations of N_{alloc} are done for both nitrogen and phosphorus. The actual allocation of carbon, nitrogen and phosphorus is set by whichever nutrient is more limiting at that timestep given the lower of the ratios N_{alloc}:N_{demand}.

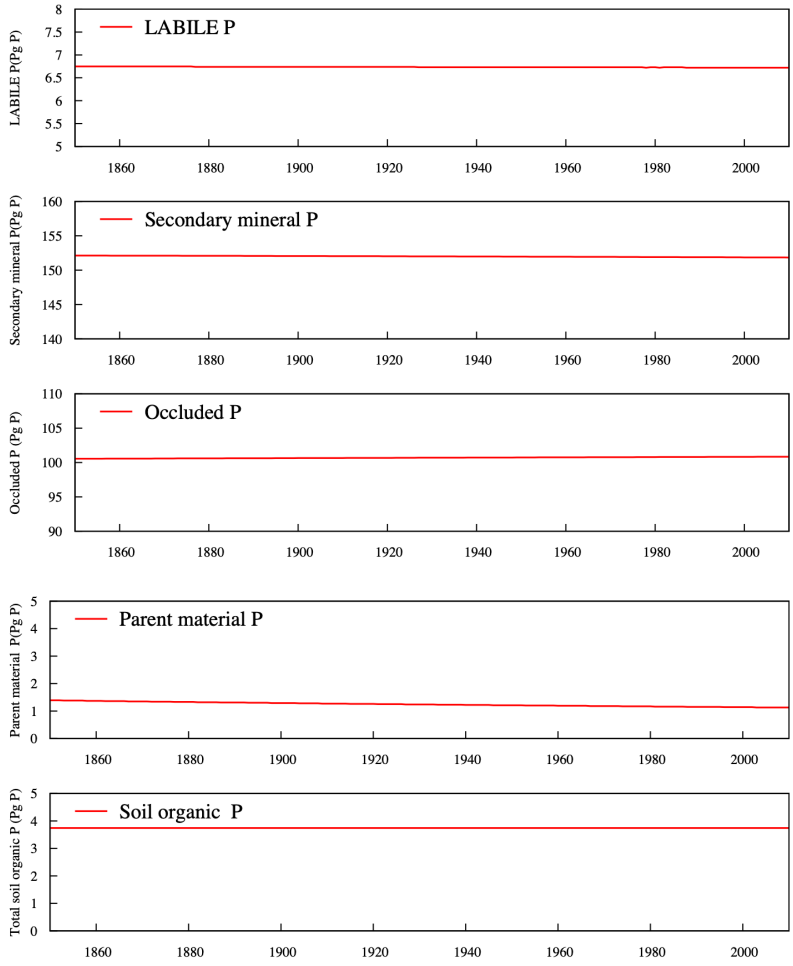

Figure S1: Time series of globally-integrated P pools for the control run, which is the continuation of the normal spinup.

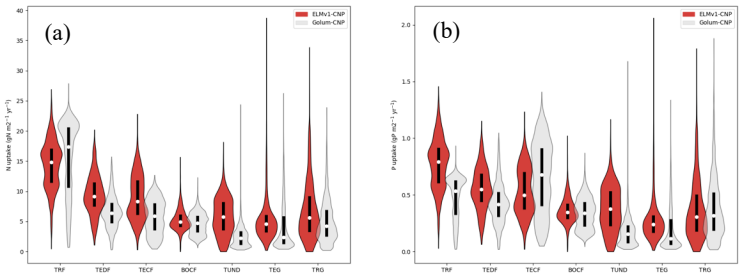

Figure S2: Violin plots of (a) nitrogen uptake (g N m^{-2} yr^{-1}) and (b) phosphorus uptake (g P m^{-2} yr^{-1}) from ELMv1-CNP and GOLUM-CNP for seven biomes: tropical rainforest (TRF), temperate deciduous forest (TEDF), temperate coniferous forest (TECF), boreal coniferous forest (BOCF), temperate grassland (TEG) and tropical grassland (TRG). Plots show the medians of all grid cells in each biome (open circles) and the probability density distribution (balloons).

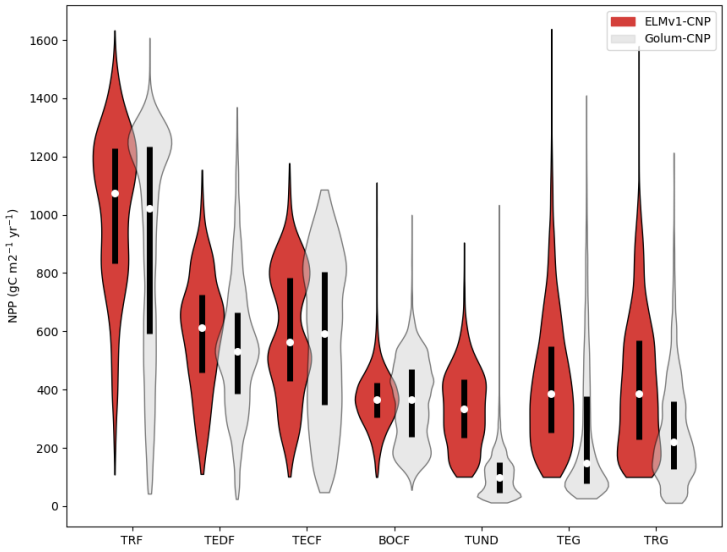

Figure S3: Violin plots of NPP (g C m^{-2} yr^{-1}) from ELMv1-CNP and GOLUM-CNP for seven biomes: tropical rainforest (TRF), temperate deciduous forest (TEDF), temperate coniferous forest (TECF), boreal coniferous forest (BOCF), temperate grassland (TEG) and tropical grassland (TRG). Plots show the medians of all grid cells in each biome (open circles) and the probability density distribution (balloons).

(a)

(b)

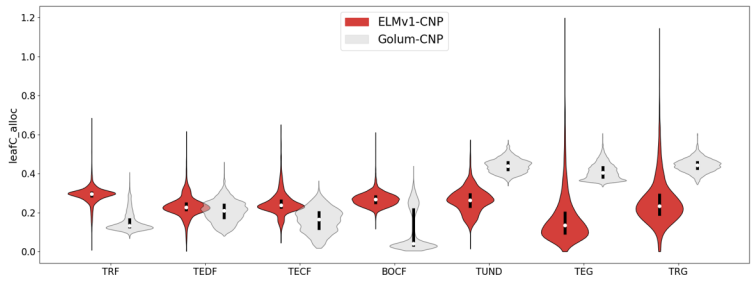

Figure S4:: Violin plots of NPP allocation fractions to leaf from ELMv1-CNP and GOLUM-CNP for seven biomes: tropical rainforest (TRF), temperate deciduous forest (TEDF), temperate coniferous forest (TECF), boreal coniferous forest (BOCF), temperate grassland (TEG) and tropical grassland (TRG). Plots show the medians of all grid cells in each biome (open circles) and the probability density distribution (balloons).

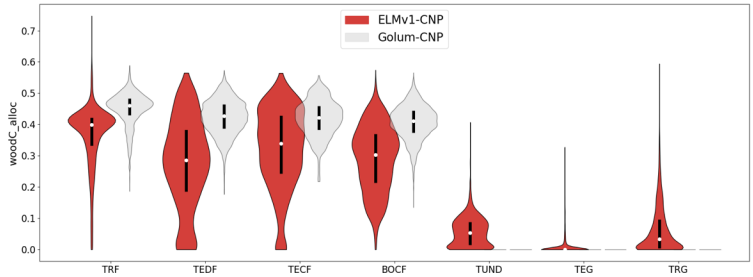

Figure S5:: Violin plots of NPP allocation fractions to wood from ELMv1-CNP and GOLUM-CNP for seven biomes: tropical rainforest (TRF), temperate deciduous forest (TEDF), temperate coniferous forest (TECF), boreal coniferous forest (BOCF), temperate grassland (TEG) and tropical grassland (TRG). Plots show the medians of all grid cells in each biome (open circles) and the probability density distribution (balloons).

Deleted: <object><object>

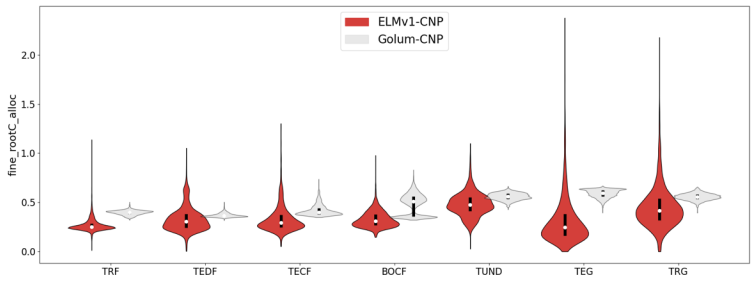

Figure S6: Violin plots of NPP allocation fractions to fine root from ELMv1-CNP and GOLUM-CNP for seven biomes: tropical rainforest (TRF), temperate deciduous forest (TEDF), temperate coniferous forest (TECF), boreal coniferous forest (BOCF), temperate grassland (TEG) and tropical grassland (TRG). Plots show the medians of all grid cells in each biome (open circles) and the probability density distribution (balloons).

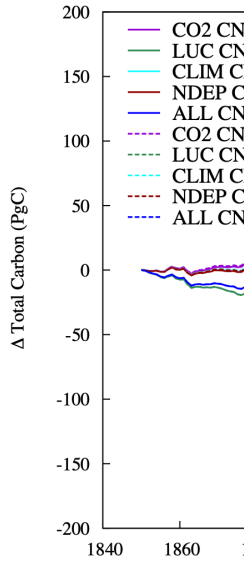

Moved down [1]:

Figure S7: Simulated change in land carbon storage in response to changes in CO2, land use and land cover change, N deposition, climate during 1850-2010. Unit: Pg C. CN is for ELMv1-CN and CNP is for ELMv1-CNP

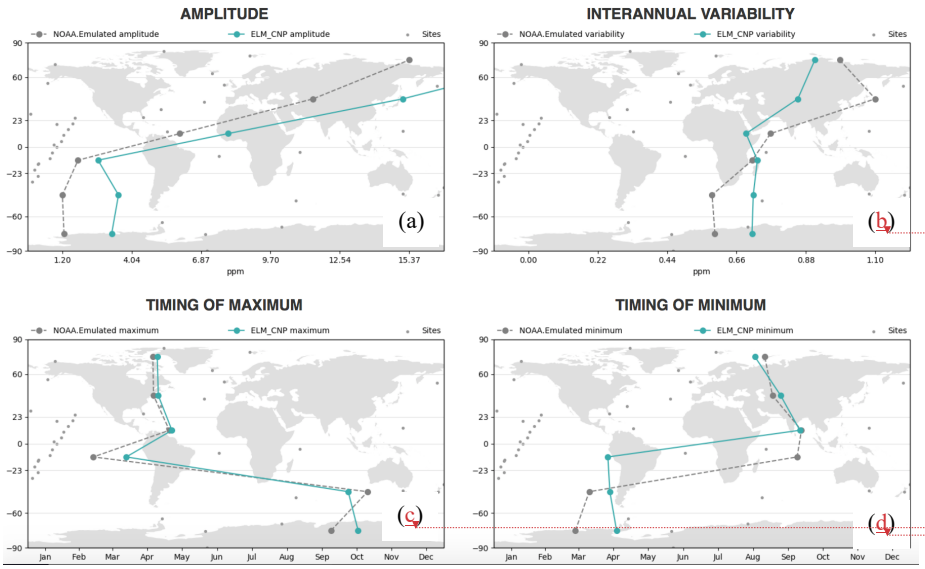

Figure S7: The comparison of atmospheric CO_2 concentrations inferred from ELM v1-CNP land-carbon fluxes (green lines) with in situ flask measurements from NOAA's global Cooperative Air Sampling Network (gray lines) in ILAMB: (a) the mean seasonal amplitude over flask sites [ppm], (b) the range of interannual variability [ppm], (c) the average month-of-year when the peak CO2 concentration occurs, and (d) the average month-of-year when the lowest CO2 concentration occurs. Observations and measurements are binned within 30◦ latitude increments; small gray dots indicate individual flask sampling locations.

Deleted: a

Deleted: a

Deleted: a

Deleted: 8

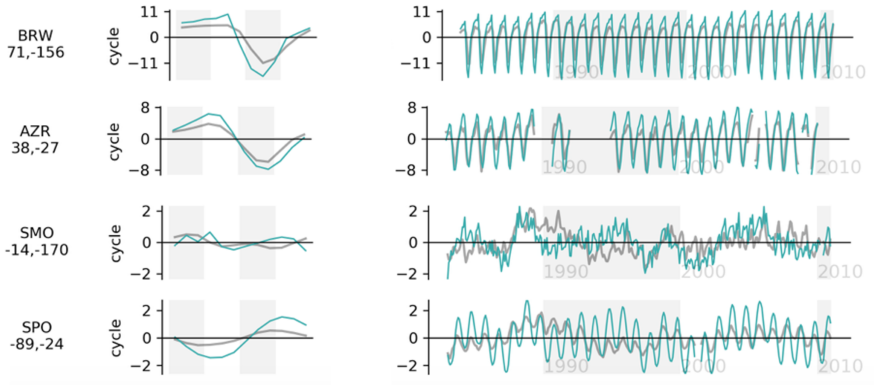

Figure S8: The comparison of atmospheric CO_2 concentrations [ppm] inferred from ELM v1-CNP land-carbon fluxes (green lines) with in situ flask measurements from NOAA's global Cooperative Air Sampling Network (gray lines) in ILAMB: Mean seasonal cycles (left) and full time series (right) for four flask sites: (d) Barrow (71° N, 156° W), (e) Azores (38° N, 27° W), (f) Samoa (14° S, 170° W), and (g) South Pole (89° S, 24° W). Grey shading in the seasonal cycle plots (left) is meant to show the magnitude of seasonality. Grey shading in the time series plots (right) is to show the decades (e.g. 1990 -2000).

Deleted: 9

Moved (insertion) [1]

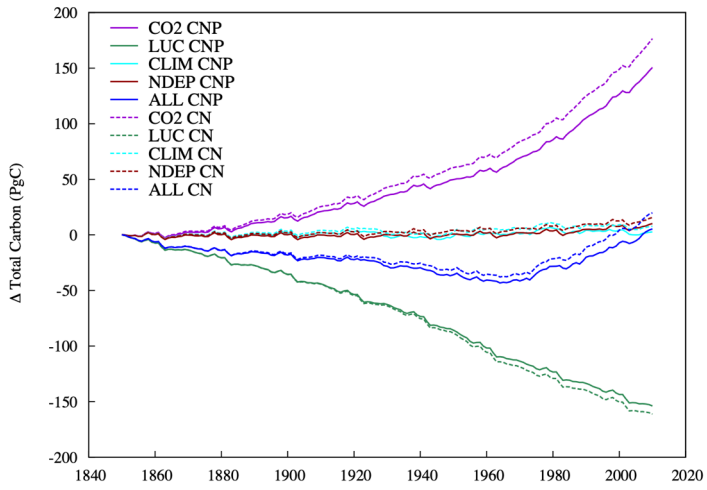

Figure S9: Simulated change in land carbon storage in response to changes in CO2, land use and land cover change, N deposition, climate during 1850-2010. Unit: Pg C. CN is for ELMv1-CN and CNP is for ELMv1-CNP

Deleted: 7

Table S1: PFT dependent parameters*

PFT	Leaf C:N	Leaf C:P	Fine root C:N	Fine root C:P	Live wood C:N	live wood C:P	Dead wood C:N	Dead wood C:P
Needleleaf evergreen tree - temperate	35	525	42	1000	50	3000	500	3000
Needleleaf evergreen tree - boreal	40	400	42	1000	50	3000	500	3000
Needleleaf deciduous tree - boreal	25	250	42	1000	50	3000	500	3000
Broadleaf evergreen tree - tropical	30	600	42	1000	50	3000	500	3000
Broadleaf evergreen tree - temperate	30	450	42	1000	50	3000	500	3000
Broadleaf deciduous tree - tropical	25	500	42	1000	50	3000	500	3000
Broadleaf deciduous tree - temperate	25	375	42	1000	50	3000	500	3000
Broadleaf deciduous tree - boreal	25	250	42	1000	50	3000	500	3000
Broadleaf evergreen shrub - temperate	30	450	42	1000	50	3000	500	3000
Broadleaf deciduous shrub - temperate	25	375	42	1000	50	3000	500	3000
Broadleaf deciduous shrub - boreal	25	250	42	1000	50	3000	500	3000
C3 arctic	25	250	42	1000				
C3 grass	25	375	42	1000				
C4 grass	25	375	42	1000				

*The sources of the parameters are provided in detail in the supporting information of Yang et al. (2016)

Table S2: Soil order dependent parameters*

	S_{max}	K_s	r_adsorp	r_desorp	r_weathering	R_occlusion
Andisol	1000	0.6	0.005	0.00022	0.005	1e-6
Gelisol	500	0.6	0.005	0.00022	0.001	1e-6
Histosol	500	0.6	0.005	0.00022	0.001	1e-6
Entisol	432	0.49	0.005	0.00022	0.001	1e-6
Inceptisol	500	0.6	0.005	0.00022	0.001	1e-6
Aridsol	700	0.3	0.005	0.00022	0.001	1e-6
Vertisol	700	0.3	0.005	0.00022	0.001	1e-6
Mollisol	700	0.3	0.005	0.00022	0.001	1e-6
Alfisol	700	0.06	0.005	0.00022	0.001	1e-6
Spodosol	925	0.03	0.005	0.00022	0.001	1e-6
Ultisol	1000	0.03	0.004	0.00022	0.0001	1e-6
Oxisol	1000	0.03	0.004	0.00022	0.0001	1e-6

*The sources of the parameters are provided in detail in the supporting information of Yang et al. (2016)

Table S3: List of Input Data

	Input data	Reference
Meteorological forcing	The Global Soil Wetness Project forcing dataset (GSWP3)	http://hydro.iis.u-tokyo.ac.jp/GSWP3/
Land use change	Land-Use harmonization data set (LUH2)	Hurtt et al., 2020
N deposition		Hegglin et al., 2016
CO_2		Meinshausen et al., 2017
P deposition		Mahowald et al. (2008)
Soil P maps	Global maps of different P pools	Yang et al. (2013)

Table S4: Observational Dataset Used for Carbon Cycle Evaluation in ILAMB

Variable	Datasets	References
Biomass	GEOCARBON	Saatchi et al.,2011
	NBCD2000	Kellndorfer et al., 2013
	USForest	Blackard et al., 2008
Burned area	GFED4S	Giglio et al., 2010
Carbon dioxide	NOAA.Emulated	Dlugokencky et al., 2020
Gross primary productivity	Fluxnet	Lasslop et al., 2010
	GBAF	Jung et al., 2011
Leaf area index	AVHRR	Myneni et al., 1997
	MODIS	De Kauwe et al., 2011
Global Net Ecosystem Carbon Balance	GCP	Le Quere et al., 2016
	Hoffman	Hoffman et al., 2014
Net ecosystem exchange	Fluxnet	Lasslop et al., 2010
	GBAF	Jung et al., 2010
Ecosystem respiration	Fluxnet	Lasslop et al., 2010
	GBAF	Jung et al., 2010
Soil carbon	HWSD	Todd-Brown et al., 2013
	NCSCDV22	Hugelius et al., 2013
	Koven	Koven et al., 2017

Deleted: e

Reference:

Blackard, J., Finco, M., Helmer, E., Holden, G., Hoppus, M., Jacobs, D., . . . Riemann, R. (2008). Mapping US forest biomass using nationwide forest inventory data and moderate resolution information. *Remote Sensing of Environment, 112*(4), 1658-1677.

De Kauwe, M. G., Disney, M., Quaife, T., Lewis, P., & Williams, M. (2011). An assessment of the MODIS collection 5 leaf area index product for a region of mixed coniferous forest. *Remote Sensing of Environment, 115*(2), 767-780.

Dlugokencky, E.J., J.W. Mund, A.M. Crotwell, M.J. Crotwell, and K.W. Thoning (2020), Atmospheric Carbon Dioxide Dry Air Mole Fractions from the NOAA GML Carbon Cycle Cooperative Global Air Sampling Network, 1968-2019, Version: 2020-07, https://doi.org/10.15138/wkgj-f215

Giglio, L., Randerson, J., Van der Werf, G., Kasibhatla, P., Collatz, G., Morton, D., & DeFries, R. (2010). Assessing variability and long-term trends in burned area by merging multiple satellite fire products. *Biogeosciences, 7*(3), 1171-1186.

Hegglin, M., Kinnison, D., & Lamarque, J.-F. (2016). CCMI nitrogen surface fluxes in support of CMIP6-version 2.0. Earth System Grid Federation. https://doi.org/10.22033/ESGF/input4MIPs.1125

Hoffman, F. M., Randerson, J. T., Arora, V. K., Bao, Q., Cadule, P., Ji, D., . . . Lindsay, K. (2014). Causes and implications of persistent atmospheric carbon dioxide biases in Earth System Models. *Journal of Geophysical Research: Biogeosciences, 119*(2), 141-162.

Hugelius, G., Bockheim, J. G., Camill, P., Elberling, B., Grosse, G., Harden, J. W., . . . Kuhry, P. (2013). A new data set for estimating organic carbon storage to 3 m depth in soils of the northern circumpolar permafrost region. *Earth System Science Data (Online), 5*(2).

Hurtt, G. C., Chini, L., Sahajpal, R., Frolking, S., Bodirsky, B. L., Calvin, K., . . . Goldewijk, K. K. (2020). Harmonization of global land-use change and management for the period 850–2100 (LUH2) for CMIP6. *Geoscientific Model Development Discussions*, 1-65.

Jung, C.-G., Shin, H.-J., Park, M.-J., Joh, H.-K., & Kim, S.-J. (2011). Evaluation of MODIS Gross Primary Production (GPP) by Comparing with GPP from CO 2 Flux Data Measured in a Mixed Forest Area. *Journal of the Korean Society of Agricultural Engineers, 53*(2), 1-8.

Kellndorfer, J., Walker, W., Kirsch, K., Fiske, G., Bishop, J., LaPoint, L., . . . Westfall, J. (2013). NACP aboveground biomass and carbon baseline data, V. 2 (NBCD 2000), USA, 2000. *ORNL DAAC*.

Koven, C. D., Hugelius, G., Lawrence, D. M., & Wieder, W. R. (2017). Higher climatological temperature sensitivity of soil carbon in cold than warm climates. *Nature Climate Change, 7*(11), 817-822.

Lasslop, G., Reichstein, M., Papale, D., Richardson, A. D., Arneth, A., Barr, A., . . . Wohlfahrt, G. (2010). Separation of net ecosystem exchange into assimilation and respiration using a light response curve approach: critical issues and global evaluation. *Global change biology, 16*(1), 187-208.

Mahowald, N., Jickells, T. D., Baker, A. R., Artaxo, P., Benitez-Nelson, C. R., Bergametti, G., . . . Herut, B. (2008). Global distribution of atmospheric phosphorus sources, concentrations and deposition rates, and anthropogenic impacts. *Global Biogeochemical Cycles, 22*(4).

Meinshausen, M., Vogel, E., Nauels, A., Lorbacher, K., Meinshausen, N., Etheridge, D. M., Fraser, P. J., Montzka, S. A., Rayner, P. J., Trudinger, C. M., Krummel, P. B., Beyerle,

U., Canadell, J. G., Daniel, J. S., Enting, I. G., Law, R. M., Lunder, C. R., O'Doherty, S., Prinn, R. G., Reimann, S., Rubino, M., Velders, G. J. M., Vollmer, M. K., Wang, R. H. J., and Weiss, R. (2017). Historical greenhouse gas concentrations for climate modelling (CMIP6), Geosci. Model Dev., 10, 2057-2116.

Myneni, R. B., Ramakrishna, R., Nemani, R., & Running, S. W. (1997). Estimation of global leaf area index and absorbed PAR using radiative transfer models. *IEEE Transactions on Geoscience and Remote Sensing, 35*(6), 1380-1393.

Yang, X., Post, W. M., Thornton, P. E., & Jain, A. (2013). The distribution of soil phosphorus for global biogeochemical modeling. *Biogeosciences, 10*(4), 2525-2537. doi:10.5194/bg-10-2525-2013.

Richardson, A. D., Carbone, M. S., Huggett, B. A., Furze, M. E., Czimczik, C. I., Walker, J. C., . . . Murakami, P. (2015). Distribution and mixing of old and new nonstructural carbon in two temperate trees. *New Phytologist, 206*(2), 590-597.

Yang, X., Thornton, P. E., Ricciuto, D. M., & Hoffman, F. M. (2016). Phosphorus feedbacks constraining tropical ecosystem responses to changes in atmospheric CO2 and climate. *Geophysical Research Letters, 43*(13), 7205-7214.